DISCLAIMER

This report was prepared as an account of work sponsored by an agency of the United States Government. Neither the United States Government nor any agency thereof, nor any of their employees, makes any warranty, express or implied, or assumes any legal liability or responsibility for the accuracy, completeness, or usefulness of any information, apparatus, product, or process disclosed, or represents that its use would not infringe privately owned rights. Reference herein to any specific commercial product, process, or service by trade name, trademark, manufacturer, or otherwise does not necessarily constitute or imply its endorsement, recommendation, or favoring by the United States Government or any agency thereof. The views and opinions of authors expressed herein do not necessarily state or reflect those of the United States Government or any agency thereof. Reference herein to any social initiative (including but not limited to Diversity, Equity, and Inclusion (DEI); Community Benefits Plans (CBP); Justice 40; etc.) is made by the Author independent of any current requirement by the United States Government and does not constitute or imply endorsement, recommendation, or support by the United States Government or any agency thereof.

Final Technical Report (FTR)

Cover Page

a. *Federal Agency*	Department of Energy Geothermal Technologies Program	
b. *Award Number*	DOE-EE0008763	
c. *Project Title*	Machine Learning Approaches to Predicting Induced Seismicity and Imaging Geothermal Reservoir Properties	
d. *Recipient Organization*	Pennsylvania State University 536 Deike Bld., University Park, PA 16802 DUNS: 00-340-3953	
e. *Project Period*	*Start:* 9/1/2019	*End:* 12/31/2024
f. *Principal Investigator (PI)*	Chris Marone Professor of Geophysics marone@psu.edu +1.814.865.7964	
g. *Business Contact (BC)*	Jennifer Lear Director of Research Administration qul48@psu.edu +1.814.865.7650	
h. *Certifying Official (if different from the PI or BC)*	PI as above	

C.J. Marone

Signature of Certifying Official

24 Mar. 2025

Date

By signing this report, I certify to the best of my knowledge and belief that the report is true, complete, and accurate. I am aware that any false, fictitious, or fraudulent information, misrepresentations, half-truths, or the omission of any material fact, may subject me to criminal, civil or administrative penalties for fraud, false statements, false claims or otherwise. (U.S. Code Title 18, Section 1001, Section 287 and Title 31, Sections 3729-3730). I further understand and agree that the information contained in this report are material to Federal agency's funding decisions and I have any ongoing responsibility to promptly update the report within the time frames stated in the terms and conditions of the above referenced Award, to ensure that my responses remain accurate and complete.

1. Acknowledgements: This material is based upon work supported by the U.S. Department of Energy's Office of Energy Efficiency and Renewable Energy (EERE) Geothermal Technologies Office (GTO) under the DE-FOA-0001956; DOE Control number: 1956-1518; Award Number DE-EE0008763

3. Executive Summary:

This project developed machine learning (ML) methods, lab data sets, and field data to advance geothermal exploration and geothermal energy production. The work had three focus areas. One involved the development of ML methods to use microearthquakes (MEQs) for imaging geothermal reservoir properties and improving subsurface characterization – most importantly the evolution of permeability within the evolving reservoir. This part of the work included development of ML approaches for automated MEQ location, focal mechanism determination and identification of earthquake precursors. The second area focused on using MEQ signals generated by geothermal exploration and production to predict the relationship between fluid injection and seismicity. Here, we extended to reservoir scale our success in using ML to predict laboratory earthquakes and fault zone stress state. The third focus area was on lab experiments. Here, we developed new ML models for lab earthquake prediction and identification of precursors to failure to improve earthquake forecasting and early warning in geothermal settings.

Major outcomes of our work include ML models that learn from MEQ signals during geothermal exploration and production to predict induced seismicity. MEQs occur naturally in connection with drilling and energy production. We developed ML methods to use the seismic waves from these events to characterize the elastic, hydraulic and poromechanical properties of reservoirs. Our work illuminated fracture geometry and the evolution of fracture permeability by incorporating seismic coda wave analysis and ML methods to relate fluid injection and seismicity. We significantly expanded laboratory earthquake prediction to include methods that use both passive measurements of microearthquakes within the lab fault zones and also active source acoustic measurements of fault zone elastic properties. These methods can now predict fault zone stress state, time to failure and the magnitude of lab earthquakes. Our work showed that repetitive stick-slip failure events during frictional sliding (the lab equivalent of earthquakes) are preceded by a cascade of micro-failure events that radiate energy in a manner that foretells unstable failure – manifest as laboratory MEQs. We documented a mapping between fracture properties and statistical attributes of elastic radiation. We extended existing works to geothermal reservoir scale and developed ML methods to determine reservoir permeability, fracture properties, and their evolution during geothermal energy production.

An attractive feature of ML algorithms is their ability to handle big datasets and reveal patterns and correlations that may remain invisible to conventional analyses. Our work connected data from field, laboratory and intermediate scales to study permeability, stress, strength, fracture stiffness and geometry. At the field scale we used data from the Newberry Volcano field site, UtahFORGE, EGS Collab, and also the Bedretto underground research lab in Switzerland. These data sets are bridging the gap between the lab scale, theory, and reservoir scale.

Our work produced plain language summaries to improve public understanding of DOE research. We also developed openly distributed ML and seismicity datasets for use by all researchers and we published connections between induced seismicity in geothermal areas and reservoir properties including permeability, fracture properties, and stress state. Our models are designed for the large data sets of induced seismicity typically associated with geothermal sites. We produced labeled event catalogs and used them on geothermal data to assess how ML can facilitate geothermal production and exploration. All datasets are available on the GDR

Productivity: The project produced 32 publications in peer reviewed journals (two are in review). It supported the work of 6 PhD students, 40 conference presentations, 6 keynote talks at national meetings, and mentoring and professional development for 4 postdoctoral fellows.

4. Table of Contents:

5. Background:

Geothermal energy production requires the formation and control of connected flow paths via hydraulic stimulation of critically stressed fractures. Fracture formation and stimulation is typically associated with microearthquakes, which generate seismic waves that can impact the topology and connectivity of the geothermal reservoir, cause damage to surface structures, and/or result in project termination. In our project we developed methods to: 1) forecast the spatiotemporal evolution of induced seismicity during geothermal energy production, 2) predict the magnitude and location of major seismic events induced during stimulation and production, with a view to mitigation, and 3) develop a better understanding of how fault zone elastic properties change during the seismic cycle so that such measurements in geothermal production settings can forecast and eventually predict impending earthquakes that could cause local damage or project termination.

An attractive feature of ML algorithms is their ability to handle big datasets and reveal patterns and correlations in large datasets that may remain invisible to conventional analyses (e.g., Masotti et al., 2006; Li et al., 2017; Mudunuru et al., 2017; Holtzman et al., 2018; Marone, 2018; Srinivasan et al., 2018; Viswanathan et al., 2018). For this project work, we employed ML methods to link data from field, laboratory and intermediate scales to study permeability, stress, strength, fracture stiffness and geometry. At field Scale we used ML to link the characteristics of historic MEQs from the Newberry Volcano field site (2014 stimulation - Fang et al., 2018) and others (Desert Peak, NV; Geysers, CA) where injection pressures and flow rates are jointly available to independently determine permeability evolution. We extended this work and further tested the models with additional studies at UtahFORGE (Yu et al., 2024a), EGS Collab (Yu et al., 2024b, 2025a), and the Bedretto Underground research lab (Yu et al., 2025b). Laboratory Scale: We used elastic waves of lab earthquakes conducted with the concurrent measurement of evolving permeability (Rivière et al., 2018; Shokouhi et al., 2018; Bolton et al., 2018; Borat et al., 2023, 2024; Affinito et al., 2024) and ML to link the features of these waveforms to independently measured features of the experiments (labquakes, permeability, stress, fracture strength, stiffness and geometry). Intermediate Scale: Here, we used the MEQ and permeability data from the EERE-sponsored EGS Collab project that involves the controlled and very closely monitored stimulation of a "geothermal" reservoir in the Sanford Underground Lab (Lead, ND). We also used unique data from the Bedretto Underground research lab and developed ML approaches to bridge the gap between the lab and field scale. A key objective was to develop labeled catalogs of seismicity (at the lab and field scale) for ML work. These catalogs are available in the GDR.

Imaging geothermal reservoirs using elastic waves from induced seismicity

Imaging geothermal reservoir properties for exploration and creating distributed permeability for production are key challenges in geothermal reservoirs. Fluid injection is a standard approach, however, it can induce seismicity and negatively impact reservoir management. To address these issues we developed ML techniques to: 1) locate induced seismicity and illuminate the geometry of permeable zones and 2) predict seismicity from fluid injection history. We began with seismic data from the 2014 EGS stimulation at the Newberry Volcano site and the 2011 EGS stimulation at the Geysers, California site (*Jeanne et al*., 2015) and extended the work to other areas. We developed ML methods to: 1) locate the events and determine magnitudes, 2) construct fracture flow models that link seismicity and reservoir permeability (e.g., *Fang et al.*, 2018). Here, seismic source properties were determined with ML and time reversal imaging (*Zhu et al.*, 2018b), which

provided rapid, high resolution source locations. We explored several approaches based on fracture-based models that relate fracture aperture and permeability. We used those to connect to the spatiotemporal evolution of reservoir elastic properties using dynamic acousto-elastic theory (*Rivière et al.*, 2016; *Shokouhi et al.*, 2017; *Jin et al.*, 2018; Wood et al., 2021).

Our work has produced a transformational advance in our understanding of reservoir imaging, induced seismicity, and earthquake prediction. Our methods have made it possible to image and track fluid plumes in underground reservoirs. Those observations have been used to illuminate the nonlinear relationship between fluid flow, seismic wave speed, and non-linear elasticity.

6. Project Objectives

Our goals were to develop ML methods to illuminate permeability structure and improve seismic safety of geothermal energy production. Our work applies to the full geothermal project lifecycle, starting with identifying and ranking drilling targets and including the installation and use of downhole sensors during technology validation.

Several hypotheses were tested:

i. ML inspired analysis of MEQs can be used to forecast (and ultimately predict) large induced seismic events and image the permeability structure of geothermal reservoirs to improve predictability of reservoir capacity and production. This hypothesis cannot be rejected based on our data.

ii. Supervised ML algorithms can be trained to identify earthquake precursors such as changes in elastic wave speed, scattering and attenuation in laboratory data and in tectonic fault settings Our data collected for this project are consistent with this hypothesis; it cannot be rejected based on our data.

iii. Unsupervised machine learning can be used to identify clusters of similar features in seismic and permeability data from active geothermal reservoirs. Our data collected for this project are consistent with this hypothesis; it cannot be rejected based on our data. We find that MEQ locations can be used to understand evolving fracture strength and permeability structure.

iv. ML algorithms can be developed to rapidly and automatically locate MEQs using seismic data from geothermal sites. These locations can illuminate flow paths and reservoir permeability structure. Our data collected for this project are consistent with this hypothesis; it cannot be rejected based on our data.

Our project work has integrated activities across disciplines and provided a high-level coordinated effort to bring ML into geothermal energy. Our work on ML with big data has shown the utility and improvements in subsurface characterization of permeability and induced seismicity based on fluid injection data. Our project has helped DOE objectives for energy production and public safety related to drilling and fluid injection.

Extending Lab Earthquake Prediction to Reservoir Scale

Objective: To develop ML approaches for forecasting (and ultimately predicting) large seismic events associated with EGS stimulation and geothermal energy production.

Expected results: Test Hypotheses *i* and *ii*. Expand the lab database for ML prediction of lab earthquakes. Apply unsupervised and supervised ML methods to seismic data from geothermal sites to test the hypotheses that: 1) large seismic events are proceeded by distinct changes in ML clusters and 2) supervised ML can be used to predict changes in seismic rate and/or large seismic events.

Imaging Geothermal Reservoir Properties Using MEQs

Objective: Develop ML methods to image geothermal reservoir properties using elastic waves from induced and natural seismicity (MEQs).

End result: We tested Hypotheses *i -iv* and developed ML techniques to locate induced seismicity, determine focal mechanisms in some cases, and illuminate the geometry of permeable zones. The outcomes and results are described below in Section 7.

7. Project Results and Discussion

Our work was done in two phases (2021-2022 and 2023-2024)

Phase 1 activities developed machine learning (ML) methods to advance geothermal exploration and geothermal energy production. We focused in two broad areas. One using field data from EGS sites (Area 1) and one using lab data (Area 2) that served as a testing ground for ML method development and process-based understanding. These **Phase 1** tasks are documented in the Gantt charts for **Phase 1**:

Area 1
1. Machine Learning to Predict Injectivity From Microearthquakes
2. Microearthquake Location Via Deep Learning and Data Fusion

Area 2
3. A Meta-learning Approach to Lab Earthquake Prediction
4. Transfer Learning for Labquakes (Active Source Seismic Monitoring)

Phase 2 activities retained the breadth of interest and expanded the topics that merge field (**Area 1**) to laboratory (**Area 2**) scales into three new focal areas applying ML/AI to key needs in deep geothermal reservoir engineering/science.

In **Phase 2** we focused on three areas:

5. ML for Seismicity-Permeability Linkage
6. ML and DL for MEQ Location
7. ML for Earthquake Prediction & Monitoring of Stress

Phase 1, Budget Period 1

Schedule of Milestones and Tasks	Year 1				Year 2			
	Q1	Q2	Q3	Q4	Q5	Q6	Q7	Q8
Task A1 ML methods to image geothermal reservoir properties using MEQ elastic waves	1.1-1.4 **MS1**	1.4-1.8	1.6-1.12 **MS3** **G/NG1**	1.10-1.11	1.11 - 1.17 **MS5**	1.12-1.18	1.14-1.17 **MS7** **G/NG3**	1.15-1.22
Task A2 ML methods to identify earthquake precursors and predict induced seismicity	2.1-2.4	2.3-2.4 **MS2**	2.4-2.9	2.8-2.10 **MS4** **G/NG2**	2.12 - 2.14	2.13-2.15 **MS6**	2.15-2.16	2.16-2.17 **MS8** **G/NG4**

Phase 2, Budget Period 2

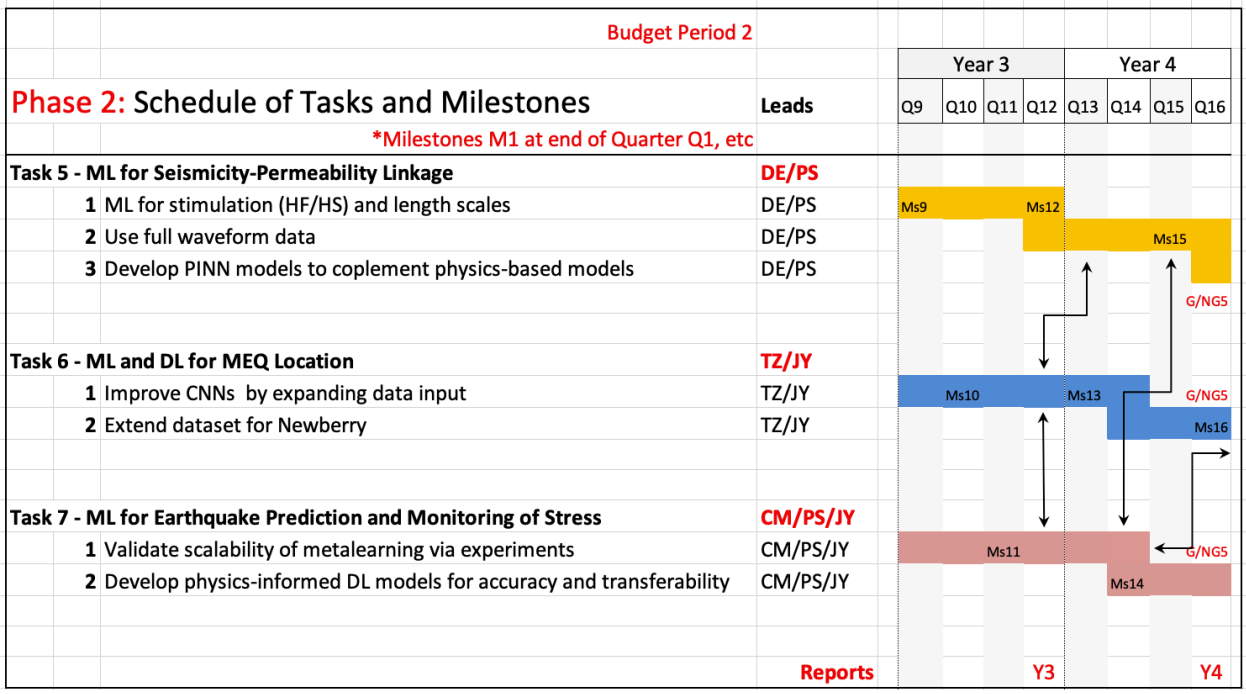

The project milestones and G/NG decision points are laid out in chronologic order.

Milestones are described in the table below. For ease of comparison between initial goals and final outcomes we list product references for each task item.

Task list with Milestones and Go-No go decision points

Area 1. ML methods to image geothermal reservoir properties using MEQ elastic waves

A1.1. Gather seismic data from geothermal operations and EGS stimulations (Leong & Zhu, 2024a,b; Yu et al., 2025ab)

A1.2. Build a local velocity model for the geothermal site if it is not available (Leong & Zhu, 2024a; Yu et al., 2023)
A1.3. Locate MEQs with standard techniques and using double difference methods (Leong & Zhu 2024a, Yu et al., 2024b; Chiaraluce et al., 2024)

MS1 will be delivery of MEQ event catalogs with preliminary locations and magnitudes based on traditional methods

MS1 was accomplished in several steps. The outcome of that work is described in the paper of Leong & Zhu, JGR, 2024.

The development of enhanced geothermal systems (EGS) hinges on accurately locating induced microearthquakes during the reservoir's stimulation process. The scarcity of microearthquake data complicates the use of traditional deep learning for this purpose. To overcome this, we developed a practical workflow, by simulating numerous synthetic data sets for training. The trained model was then applied to real-world EGS microearthquake data. We created a realistic geological model of the Newberry EGS site and generated many artificial microearthquake data for deep learning training. During the application on field data from 2012 to 2014 stimulation, the computer model successfully identified the depth and location of microearthquakes. Our results match well with what we already know about the underground structure, such as the presence of natural fractures in the rock. We showed that our approach can effectively predict microearthquake locations even when presented with limited earthquake data for training, which is promising for monitoring and improving EGS operations in the future.

A1.4. Gather lab experiment data on fracture flow, frictional strength, and elastic properties. (Affinito et al., 2024; An et al., 2024; Bolton et al., 2020, 2021, 2022, 2023; Cebry et al., 2022; den Hartog et al., 2023; Noël et al., 2024; Pignalberi et al., 2024; Shreedharan et al., 2021a,b, 2022; Wood et al., 2021, 2024)
A1.5. Analyze lab data to determine elastic wave speed, attenuation, fracture flow and permeability (Affinito et al., 2024; Bolton et al., 2020, 2021, 2022, 2023; Shreedharan et al., 2021a,b, 2022; Wood et al., 2021, 2024)
A1.6. Build event catalogs for lab earthquakes (Bolton et al., 2020, 2021, 2022, 2023; Shreedharan et al., 2021a,b, 2022)
A1.7. Build feature list for lab acoustic data and set up for supervised ML to locate lab earthquakes (Bolton et al., 2020, 2021, 2022, 2023; Shreedharan et al., 2021a,b, 2022; Jaspereson et al., 2021; Laurenti et al., 2022)
A1.8. Develop/test/apply ML methods to locate lab earthquake (Shreedharan et al., 2021b; Bolton et al., 2022)
A1.9. Automated methods to pick arrivals, catalog events, and build labeled lab and field data (Bolton et al., 2020; Yu et al., 2024b)
A1.10. Build feature list for field seismic data and prepare to use ML methods to locate MEQs (Leong & Zhu, 2024; Leong et al., 2024)
A1.11. Perform supervised ML for events location and focal mechanism solutions for MEQs (Leong & Zhu, 2024; Leong et al., 2024)
A1.12. Set up HyM-TRI and CNN to locate MEQ and determine moment tensor solutions (Leong & Zhu, 2024; Leong et al., 2024)

(Note that MS2 is part of A2 below)

MS3 will be delivery of ML methods for MEQ locations and moment tensor solutions along with a full event catalog

Conventional earthquake location methods involve iteratively minimizing the difference between picked P- and/or S-wave first arrival times and predicted data at multiple seismic stations. While these methods have been widely employed in seismology, they have limitations. The accuracy of earthquake location estimates can be affected by convergence issues, particularly when the initial location guess is not sufficiently close to the true hypocenter, the solution may converge at a local minimum, leading to inaccurate location estimates. Additionally, conventional methods can be computationally intensive, particularly when applied to large data sets or in regions with complex geology (local heterogeneities). As such, most location algorithms rely on one-dimensional (1D) velocity models, where the velocity changes only with depth. Furthermore, waveform-based methods that are based on time-reversal imaging principles utilize finite difference to compute time-reversed seismograms and the actual source location is determined by identifying the point of highest energy concentration. Wavefield simulation method is unsurprisingly computationally expensive, and the energy focusing can be ambiguous for noisy data and very heterogeneous models. Waldhauser and Ellsworth (2000) proposed hypoDD, a widely used location inversion method that iteratively minimizes the misfit between theoretical and observed differential travel-times for pairs of earthquakes (double-difference) at each station. Nonetheless, the system can get very large if all event pairs are used in double-difference methods and reducing the efficiency of location estimation.

Deep learning (DL) techniques have been increasingly applied in earthquake seismology. For example, DL has seen significant developments in earthquake event phase detection, phase picking, phase association, and integrated earthquake monitoring workflow. For DL-based earthquake location inversion, a large majority of studies rely heavily on training with labeled field data. Perol et al. (2018) used convolutional neural network (CNN) that trained on ~2,900 single station events near Guthrie, Oklahoma, in which the CNN accepts three-component waveforms and predicts earthquake location groups of six clusters. Later studies improved the earthquake location inversion method by employing more advanced DL algorithms and utilize multi-station three-component waveforms as input to predict three-dimensional (3D) locations.

We developed a machine learning workflow using a probabilistic multilayer perceptron (PMLP) to accurately predict MEQ locations from waveform data. The workflow encompasses three parts. First, we use a high-resolution 3D velocity model to simulate numerous synthetic MEQ events using 3D acoustic finite-difference modeling. From the synthetic waveforms, we extract its first arrivals. In practice, since we do not have the MEQs event origin time, we compute the cross-correlation of the first arrivals such that the first arrival of the master trace is at zero time lag. The time lags at other receivers contain the same moveout pattern as the first arrivals. Second, we train a PMLP that inputs cross-correlation time lags and outputs the locations (x, y, z) of MEQs. Lastly, we apply the trained PMLP onto the field data set to obtain field MEQ location predictions. We are essentially allowing the neural network to train on realistic or physics-informed synthetic data set, and then apply its knowledge learned onto field waveforms to predict the induced MEQ locations. Our method works well and all MEQ locations and moment tensor solutions are available in the GDR.

A1.13. Refine ML models for location and moment tensor solutions (Leong & Zhu, 2024; Leong et al., 2024)
A1.14. Construct unsupervised ML methods for location/focal mechanism cluster analysis (Leong & Zhu, 2024; Leong et al., 2024)
A1.15. Construct fracture flow models that link seismicity and reservoir permeability (Yu et al., 2023; 2024a,b,c,2025a,b)
A1.16. Gather flow and operations data from Newberry Volcano site and Geysers, California (Leong & Zhu, 2024)
A1.17. Set up Safe Reinforcement Learning (SRL) approach to work with flow and operations data (we used another approach, as described for MS5 and thus this task was not completed with SRL)

(Note that MS4 is part of A2 below)
MS5 will be delivery of fracture flow models and SRL method to optimize geothermal field operation

The distribution of permeabilities in the shallow crust are known to diminish as a power law with depth. This is driven by both the extreme sensitivity of fracture permeability to increasing stress and the rapidity with which damage occasioned by tectonic strains will heal and seal. Both stress and temperatures increase with depth. The attempt to create a fluid transmissive crust for the recovery of energy or fuels typically relies on reactivating existing fractures in shear or fracturing in tension – each mode of hydraulic-shearing or hydraulic-fracturing driven by artificially elevated fluid pressures. These modes of permeability creation result from frictional reactivation and/or brittle fracture of the crust and are typically accompanied by micro-earthquakes (MEQs).

For the work related to MS5, we link changes in crustal permeability to informative features of MEQs using two field hydraulic stimulation experiments where both MEQs and permeability evolution are recorded simultaneously. The Bidirectional Long Short-Term Memory (Bi-LSTM) model effectively predicts permeability evolution and ultimate permeability increase. Our findings confirm the form of key features linking the MEQs to permeability, offering mechanistically consistent interpretations of this association. Transfer learning correctly predicts permeability evolution of one experiment from a model trained on an alternate dataset and locale, which further reinforces the innate interdependency of permeability-to-seismicity. Models representing permeability evolution on reactivated fractures in both shear and tension suggest scaling relationships in which changes in permeability (Δk) are linearly related to the seismic moment (M) of individual MEQs as $\Delta k / M$. This scaling relation rationalizes our observation of the permeability-to-seismicity linkage, contributes to its predictive robustness and accentuates its potential in characterizing crustal permeability evolution using MEQs

A1.18. Develop/test Safe Reinforcement Learning methods to predict injection/flow/production. (we used another approach, as described for MS5 and thus this task was not completed with SRL)
A1.19. Perform supervised ML to locate high permeability zones and image flow (Yu et al., 2023; 2024a,b,c,2025a,b)
A1.20. Refine ML models and explore other ML algorithms (Yu et al., 2023; 2024a,b,c,2025a,b)
A1.21. Construct unsupervised ML methods for reservoir flow and permeability (Yu et al., 2023; 2024a,b,c,2025a,b)

A1.22. Prepare for technology validation in Budget Period 2 (done as part of MS7)

MS7 will be delivery of unsupervised ML methods for reservoir flow and permeability

This work was done as part of several studies and is described in MS5 (Yu et al., 2023; 2024a,b,c,2025a,b)

Area 2. ML methods to identify earthquake precursors and predict induced seismicity

A1.23. Build catalog of lab earthquakes (Bolton et al., 2020, 2021, 2022, 2023; Shreedharan et al., 2021a,b, 2022)

A2.1. Build feature list for supervised ML to predict time of lab earthquakes (Bolton et al., 2020, 2021, 2022, 2023; Jaspereson et al., 2021; Laurenti et al., 2022)

A2.2. Develop/test supervised ML to predict lab earthquakes; verify ML model performance (Bolton et al., 2020, 2021, 2022, 2023; Jaspereson et al., 2021; Laurenti et al., 2022; Borat et al., 2023, 2024)

A2.3. Analyze lab acoustic data to identify precursors to lab earthquakes and build a labeled catalog for ML (Bolton et al., 2020, 2021, 2022, 2023; Shreedharan et al., 2021a,b, 2022)

MS2 will be delivery of results for lab earthquake prediction

Machine learning (ML) represents a set of statistical techniques often used for predictive modeling of large data sets. We developed ML methods and applied them to a series of laboratory experiments where we generate slow and fast “earthquakes” in the lab. These laboratory experiments include systematic collection of mechanical (shear stress variations) and ultrasonic (transmitted and received high-frequency) pulses throughout multiple lab seismic cycles. By training on the ultrasonic data, we were able to predict the mechanically determined shear stress evolution, time remaining to the next labquake, and time elapsed since a previous labquake to a high-degree of accuracy. Moreover, the ML models predicting shear stress and time remaining until the next labquake improved in accuracy closer to failure. Since the ultrasonic data are thought to represent the evolution of elastic and plastic deformation at a microscopic asperity-scale, the ML process implicitly incorporates the physics of contact deformation, and provides a physical basis for the success of predictions. Our results show that these ML-based methods coupled with active seismic monitoring of faults in nature may be useful for inferring the state of stress and failure state of faults that may host earthquakes.

A2.4. Build ML methods to identify precursors to lab earthquakes (Bolton et al., 2020, 2021, 2022, 2023; Jaspereson et al., 2021; Laurenti et al., 2022; Borat et al., 2023, 2024)

A2.5. Set up automated methods to identify precursors to earthquakes in geothermal sites. (existing data were not sufficient to complete this task)

A2.6. Build feature list for ML to identify precursors for lab earthquakes. (Bolton et al., 2020, 2021, 2022, 2023; Shreedharan et al., 2021a,b, 2022)

A2.7. Build feature list for ML to identify precursors and calculate features from seismic signals in geothermal sites. (existing data were not sufficient to complete this task)

A2.8. Test supervised ML methods to identify precursors to lab earthquakes Bolton et al., 2020, 2021, 2022, 2023; Shreedharan et al., 2021a,b, 2022)

A2.9. Test supervised ML methods to identify precursors to MEQs in geothermal sites (existing data were not sufficient to complete this task)

MS4 will be delivery of ML based identification of precursors to lab earthquakes

We developed ML methods based on lab data and active-source lab seismic data, which probe asperity-scale processes, with ML methods. We showed that elastic waves passing through the lab fault zone contain information that can predict the full spectrum of labquakes from slow slip instabilities to highly aperiodic events. The ML methods utilize systematic changes in P-wave amplitude and velocity to accurately predict the timing and shear stress during labquakes. The ML predictions improve in accuracy closer to fault failure, demonstrating that the predictive power of the ultrasonic signals improves as the fault approaches failure. Our results demonstrate that the relationship between the ultrasonic parameters and fault slip rate, and in turn, the systematically evolving real area of contact and asperity stiffness allow the gradient boosting algorithm to "learn" about the state of the fault and its proximity to failure. Broadly, our results demonstrate the utility of physics-informed ML in forecasting the imminence of fault slip at the laboratory scale, which may have important implications for earthquake mechanics in nature.

A2.10. Refine ML model for precursors and explore RNN-GP models for reservoir scale data (existing data were not sufficient to complete this task)
A2.11. Construct unsupervised ML methods for cluster analysis of earthquake precursors in geothermal sites (existing data were not sufficient to complete this task)
A2.12. Set up for lab experiments under true triaxial load conditions with fluid injection, shear and seismic monitoring (Wood et al., 2021, 2024)
A2.13. Experiments to monitor fracture permeability and elastic properties with shear (Wood et al., 2021, 2024)

MS6 will be delivery of results related to ML based identification of precursors to MEQs from a geothermal site

Part of this was done in these papers: Yu et al., 2023; 2024a,b,c,2025a,b and other aspects could not be completed because existing data were not sufficient to complete this task.

A2.14. Refine ML model for earthquake prediction and explore other ML algorithms (Bolton et al., 2020, 2021, 2022, 2023; Jaspereson et al., 2021; Laurenti et al., 2022; Borat et al., 2023, 2024)
A2.15. Construct unsupervised ML methods for cluster analysis of the seismic cycle, earthquake precursors, and earthquake prediction. (existing data were not sufficient to complete this task)
A2.16. Construct safe reinforcement learning (RL) algorithms to optimize the operation of geothermal energy production while ensuring seismic safety. (existing data were not sufficient to complete this task

MS8 will be delivery of unsupervised ML techniques for A2.12 and A2.16 along with SRL results for A2.17
Part of this was done in these papers: Yu et al., 2023; 2024a,b,c,2025a,b and other aspects could not be completed because existing data were not sufficient to complete this task.

Additional results for Phase 1 work and results for Phase 2 work are described in several highlights below

Highlight 1: ML and transfer learning models for permeability evolution during fluid injection. Using microearthquakes to forecast permeability evolution and seismic moment release of induced earthquakes.
Highlight 2: Development of Deep Learning Models to Recover Permeability Evolution from Fluid-Induced Microearthquakes for Hectometer-scale Stimulations
Highlight 3: Scaling Relationships Between Seismic Moment and Permeability Changes During Shear Reactivation: Insights from Laboratory to Field-Scale Observations
Highlight 4: ML models for predicting seismicity and magnitude rate from injection features
Highlight 5: DASEventNet—A Deep Learning Model for MEQ Detection in DAS Data
Highlight 6: DASEventLocNet—A Physics-Informed Transformer for MEQ Localization with DAS Data
Highlight 7: Acoustic energy release during the laboratory seismic cycle: Insights on laboratory earthquake precursors and prediction.
Highlight 8: Predicting lab earthquakes using physics-informed neural networks and fault zone acoustic monitoring

Task 5. ML for Seismicity-Permeability Linkage

SubTask 5.1 – ML stimulation and (HF/HS) and examine length-scales.

1. Develop ML models for HydroFracture and HydroShear stimulation modes. **MS9**
2. Incorporate into DFNs and inverse models for EGS Collab.
3. Introduce various learning strategies to identify structure in datasets across scales. **MS12**

SubTask 5.2 – Use full waveform data.

1. Develop ML methods to rapidly define Moment Tensor (MT) solutions from MEQs.
2. Use full waveform and automatic feature extraction to extract key features.
3. Compare hand-picked and full waveform signatures, perm-maps & transferability. **MS15**
4. Use EGS-Collab and PoroTomo inversion-derived perm-maps and link waveform data.

Our work and results for Task 5 are described in Highlights 1-4 below.

Task 6. ML and DL or MEQ Location

SubTask 6.1 – Improve CNNs by expanding data input

1. Test regularized waveforms and use different station layouts and optimize loss function. **MS10**
2. Determine how errors in training data/labels impact location estimates. **MS 13**

SubTask 6.2 – Use addition data for Newberry and extend the approach

1. Use Newberry data for the period 09/2014-12/2014. **MS16**
2. Extend the approach to Collab & PoroTomo

Our work and results for Task 6 are described in Highlights 5 and 6 below.

Task 7. ML for Earthquake Prediction and Monitoring of Stress

SubTask 7.1 – Validate scalability of metalearning via experiments

1. Apply meta-learning to LSTM models with lab data - verify versatility of model.
2. Design new experiments to expand the range of fracture roughness, including natural fractures, and temperature. **MS11**
3. Validate effectiveness of meta-learning on earthquake prediction and stress monitoring using EGS-Collab, PoroTomo and UtahFORGE datasets.

SubTask 7.2 – Develop physics-informed DL models for accuracy and transferability

1. Incorporate fundamental laws of physics and fault rheology into the architecture of neural networks to constrain model predictions. **MS14**

Our work and results for Task 7 are described in Laurenti et al., 2024, Borat et al., 2023, 2024 and Highlights 7 and 8 below. In addition, the following are important results of our work.

Predicting failure in solids has broad applications including earthquake prediction which remains an unattainable goal. However, recent machine learning work shows that laboratory earthquakes can be predicted using micro-failure events and temporal evolution of fault zone elastic properties. Remarkably, these results come from purely data-driven models trained with large datasets. Such data are equivalent to centuries of fault motion. In addition, the underlying physics of such predictions is poorly understood. In our work, reported in Borat et al. 2023) we addressed scalability using a novel Physics Informed Neural Network (PINN). Our model encodes fault physics in the deep learning loss function using time-lapse ultrasonic data. PINN models outperform data-driven models and significantly improve transfer learning for small training datasets and conditions outside those used in training. Our work suggests that PINN offers a promising path for machine learning-based failure prediction and, ultimately for improving our understanding of earthquake physics and prediction.

Milestone Summary: Note that Milestone **MS1** corresponds to the close of **Q1**, etc., and that the relevant tasks are also noted on the WBS.

Task	Task Title	Description of Completion	Timing
Y1		**PHASE 1**	**(MS1=Q1)**
	A1.3	Deliver MEQ event catalogs based on traditional methods	**MS1**
	A2.4	Delivery of results for lab earthquake prediction	**MS2**
	A1.12	Delivery of ML methods for MEQ locations and MT solutions \	**MS3**
	A2.10	Delivery of ML based identification of precursors to lab earthquakes \	**MS4**
Y2			
	A1.17	Delivery of fracture flow models and SRL method to optimize geothermal field operation	**MS5**
	A2.14	Delivery of results related to ML based identification of precursors to MEQs from a geothermal site	**MS6**
	A1.22	Delivery of unsupervised ML methods for reservoir flow and permeability \	**MS7**
	A2.17	Delivery of unsupervised ML techniques and SRL results	**MS8**

Task	Task Title	Description of Completion	Timing
		End of project goals and plans for Phase 2	**G/NG1**
Y3		**PHASE 2**	
	5.1.1	Develop ML models for HF and HS stimulation modes.	**MS9**
	6.1.1	Test regularized waveforms and use different station layouts and optimize loss function.	**MS10**
	7.1.2	Design new experiments to replicate fracture roughness at temperatures.	**MS11**
	5.1.3	Introduce various learning strategies to identify structure in datasets across scales.	**MS12**
Y4			
	6.1.2	Determine how errors in the training data (labels) impact location estimates.	**MS13**
	7.2.1	Incorporate fundamental laws of physics and fault rheology into the architecture of neural networks to constrain model predictions.	**MS14**
	5.2.3	Compare hand-picked and full waveform signatures, perm-maps & transferability.	**MS15**
	6.2.1	Test data over the period 09/2014-12/2014. **End of project goals and plans for Phase** 3	**MS16** **G/NG2**

End of Project Goal: Deliver ML approaches for predicting induced seismicity and imaging geothermal reservoir properties along with results of testing the approaches at geothermal sites. The project-wide SMART (**S**pecific, **M**easurable, **A**chievable, **R**elevant, and **T**imely) technical achievements were: 1) the specific ML algorithms (code and description) and the test/verification results showing how the ML approaches compare to standard methods to locate MEQs, solve for moment tensor solutions, and identify earthquake precursors, and 2) the specific ML algorithms (code and description) for Safe RL of geothermal site operations and identification of reservoir flow/permeability zones.

Highlight 1: ML and transfer learning models for permeability evolution during fluid injection. Using microearthquakes to forecast permeability evolution and seismic moment release of induced earthquakes.

We developed Bi-LSTM models to predict permeability changes for both the EGS Collab and Utah FORGE datasets by leveraging features derived from microearthquake (MEQ) data (i.e., seismicity rates and cumulative seismic moments). A sample-by-sample normalization scheme was employed to safeguard against any inadvertent information leakage from validation and testing datasets, thus ensuring robust model performance. Additionally, a physics-informed loss function was introduced to impose a monotonically increasing trend in predicted permeability, reflecting the underlying physical behavior observed in hydraulic stimulations. This work is described in the papers by Yu et al., 2024a, 2024b and 2024c, and by those of Leong and Zhu (2024) and Leong et al., 2024.

Our trained Bi-LSTM model achieved high coefficients of determination (R^2) for both the EGS Collab and Utah FORGE datasets. As illustrated in Figure 1, the model's predictions closely mirrored the observed permeability evolution over time, demonstrating excellent predictive accuracy for the ultimate permeability. Although minor discrepancies occasionally arose in the intermediate time history, the overall fidelity of the predictions attests to the efficacy of the physically constrained loss function.

To further evaluate the model's generalizability, we implemented a transfer learning strategy. Specifically, the Utah FORGE Bi-LSTM model was applied to the EGS Collab dataset, and vice versa. In Figure 2A, the EGS Collab transfer learning model provided strong predictive performance for validation (Episode 4) and test (Episode 5) sets, with R^2 values of 0.91 and 0.80, respectively. A similar level of accuracy was observed when transferring the EGS Collab model to the Utah FORGE dataset (Figure 2B). Both transfer learning models accurately predicted the ultimate permeability, underscoring their capacity to capture the governing physics across different sites.

Moreover, we developed theoretical models to describe permeability evolution on reactivated fractures undergoing either shear or tension, which revealed a linear scaling relationship between permeability changes (Δk) and the seismic moment (M). This scaling relation, $\Delta k \propto M$, supports our empirical observations of a direct link between seismicity and permeability, offering further validation for using MEQ data to characterize crustal permeability evolution. These findings demonstrate the promise of combining machine learning, transfer learning, and physics-based constraints to enhance permeability prediction and advance our understanding of seismic moment–permeability mechanism.

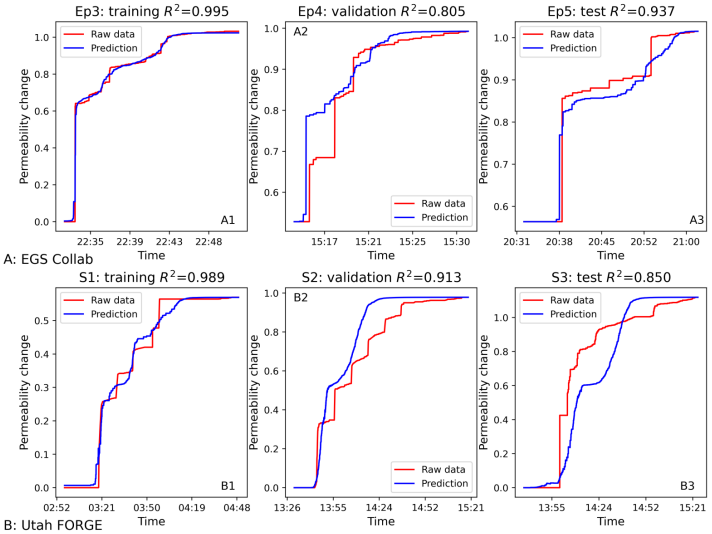

Fig. 1. Comparison between raw permeability data and predictions from training, validation and test sets for EGS-Collab and Utah FORGE datasets, respectively. The top row shows the EGS Collab Bi-LSTM model compared with raw data using Ep3 for training (A1), Ep4 for validation (A2) and Ep5 for testing (A3). The second row shows the Utah FORGE Bi-LSTM model compared with raw data using Stage 1 for training (B1), Stage 2 for validation (B2) and Stage 3 for testing (B3). (Yu et al., 2024a and 2024b)

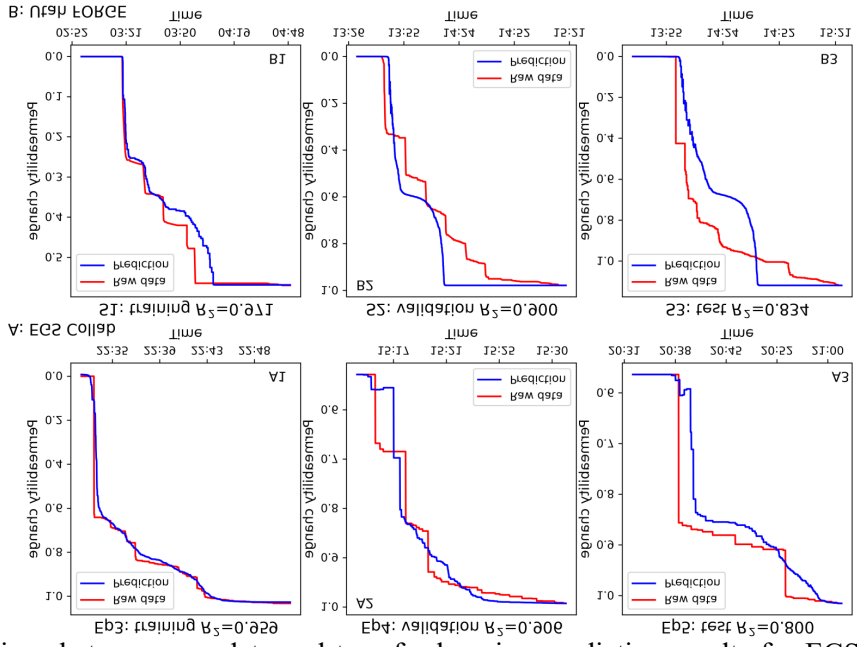

Fig. 2 Comparison between raw data and transfer learning prediction results for EGS-Collab and Utah FORGE datasets, respectively. Top row shows the results of transfer learning applied to the EGS Collab dataset results using the Utah FORGE Bi-LSTM model. Second row shows the results of transfer learning applied to the Utah FORGE dataset results comparison using the EGS Collab Bi-LSTM model. Note that the predictions are quite good for both cases of transfer learning. (Yu et al., 2024a and 2024b)

Highlight 2: Development of Deep Learning Models to Recover Permeability Evolution from Fluid-Induced Microearthquakes for Hectometer-scale Stimulations

In this work, we employed Bi-LSTM deep learning (DL) models to reconstruct the evolution of permeability during hectometer-scale hydraulic stimulations at the Bedretto Underground Laboratory. We investigated both low-volume (Phase 1) and high-volume (Phase 2) injection experiments, demonstrating that the proposed DL framework is broadly generalizable across a wide range of injection volumes. By integrating injection rate and pressure time histories with key features derived from the microearthquake (MEQ) record—namely, seismicity rates and the logarithm of cumulative seismic moment—our models successfully inferred permeability changes even for previously unseen datasets. The work is described in Yu et al., 2025.

Specifically, a Bi-LSTM model trained on low-volume stimulations in Phase 1 (Figure 3) with relatively sparse seismicity and limited permeability enhancement was able to accurately predict permeability evolution for subsequent variable-volume injections in Phase 2 (Figure 4), despite these injections having a higher seismicity rate and greater overall permeability change. Notably, the DL model also exhibited robust predictive capabilities when trained and tested directly on Phase 2 stimulations alone. In most cases, it effectively captured both the ultimate permeability magnitude at peak stimulation overpressures and the progression to that peak value. Minor discrepancies in the inferred time histories arose primarily when the pressure front expanded into heterogeneous structural domains, underscoring how geological complexity can challenge model fidelity.

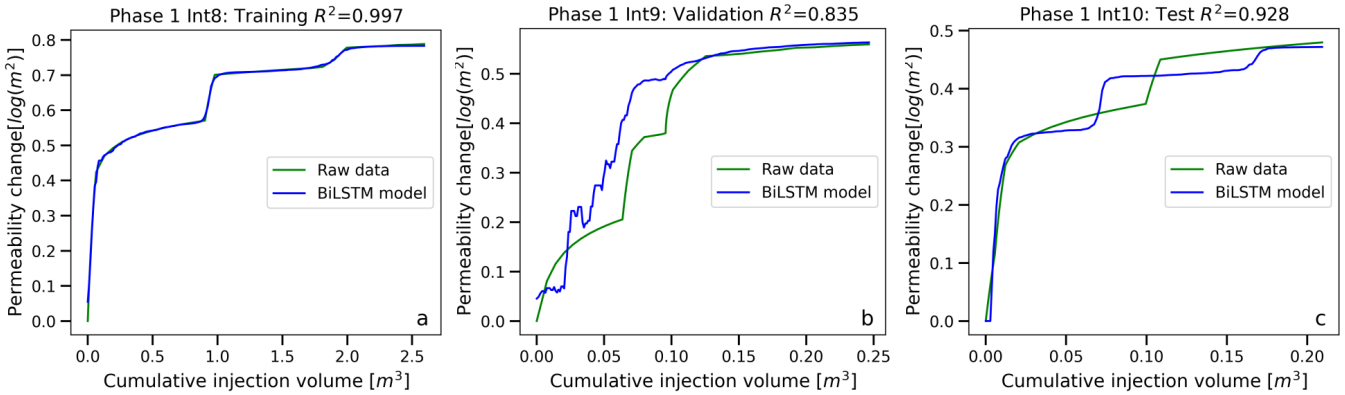

Fig. 3. Comparison between raw permeability data (ground truth) and Bi-LSTM model predictions for training, validation, and test sets using Phase 1 stimulation datasets for Intervals 8, 9, and 10, respectively. Each panel shows model output compared to raw data: (a) Interval 8 (training), (b) Interval 9 (validation), and (c) Interval 10 (testing). Note, the RMSE values for the training, validation, and testing predictions are 0.011, 0.103, and 0.060 respectively. Yu et al., 2025.

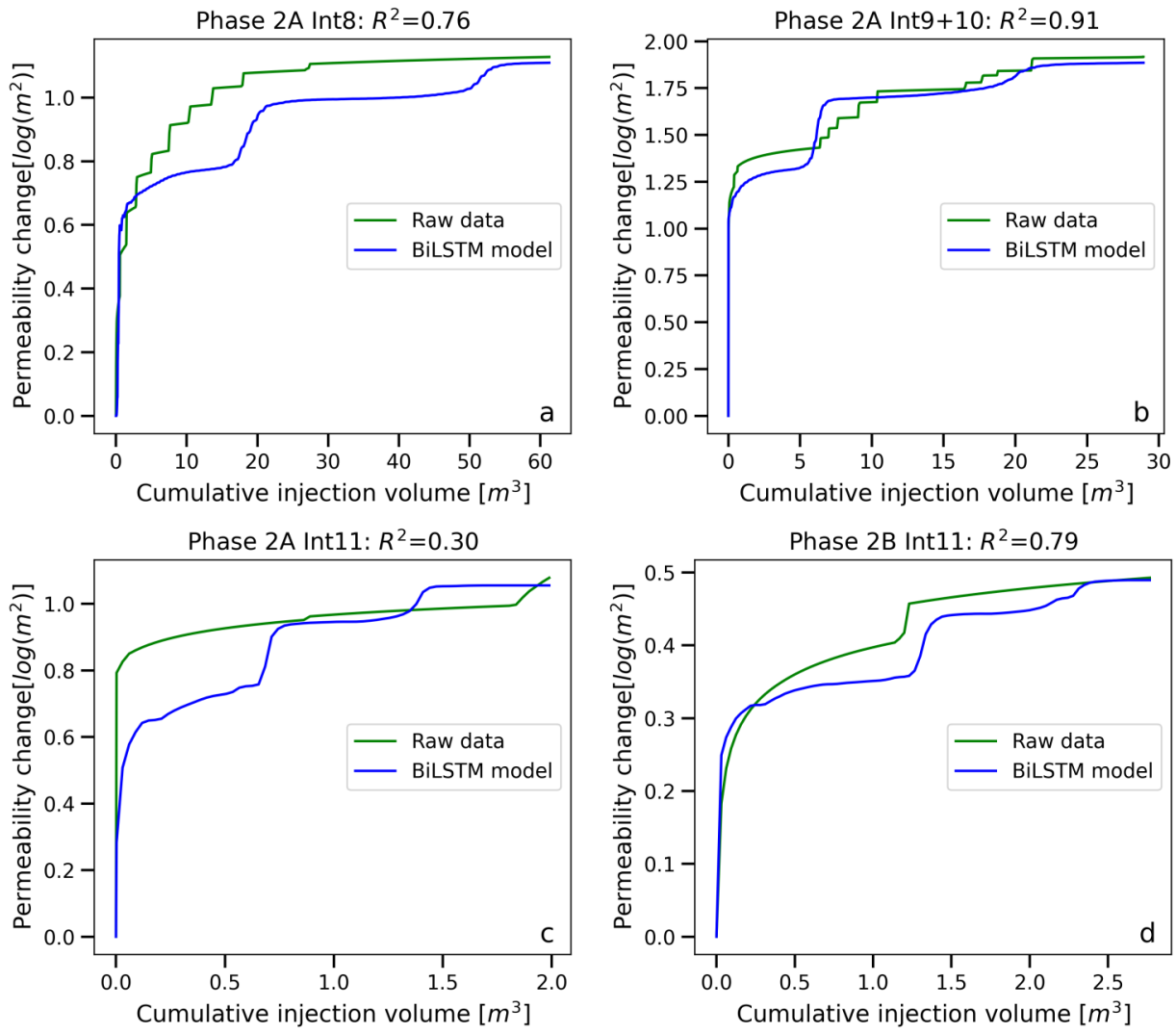

Fig. 4. Comparison between raw permeability data (ground truth) and Bi-LSTM model predictions for Phase 2 stimulations. Each panel compares model output to raw data: (a) Phase 2A Interval 8, (b) Phase 2A Interval 9+10, (c) Phase 2A Interval 11, and (d) Phase 2B Interval 11. Note, the RMSE values for the Phase 2A Interval 8, Phase 2A Interval 9+10, Phase 2A Interval 11, and Phase 2B Interval 11 predictions are 0.098, 0.036, 0.107, and 0.077 respectively. Yu et al., 2025.

In addition to quantifying permeability enhancements during peak stimulation, we performed an analysis of stress-dependent permeability reduction as injection pressures returned to background levels. The observed retreat in permeability was proportional to the reduction in stimulation pressure and was notably consistent across diverse structural domains (Figure 5). This consistency highlights the potential to infer post-stimulation permeability from peak injection data, providing an avenue for enhancing long-term reservoir management. Variations in this scaling behavior are attributed to differences in the sampled structural domains and the increased likelihood of traversing multiple domains at larger injection volumes.

Overall, these findings underscore the strong generalizability and robustness of Bi-LSTM–based DL models for capturing permeability evolution under variable injection volumes and geological complexities. The results are currently under review in *Geophysical Research Letters*.

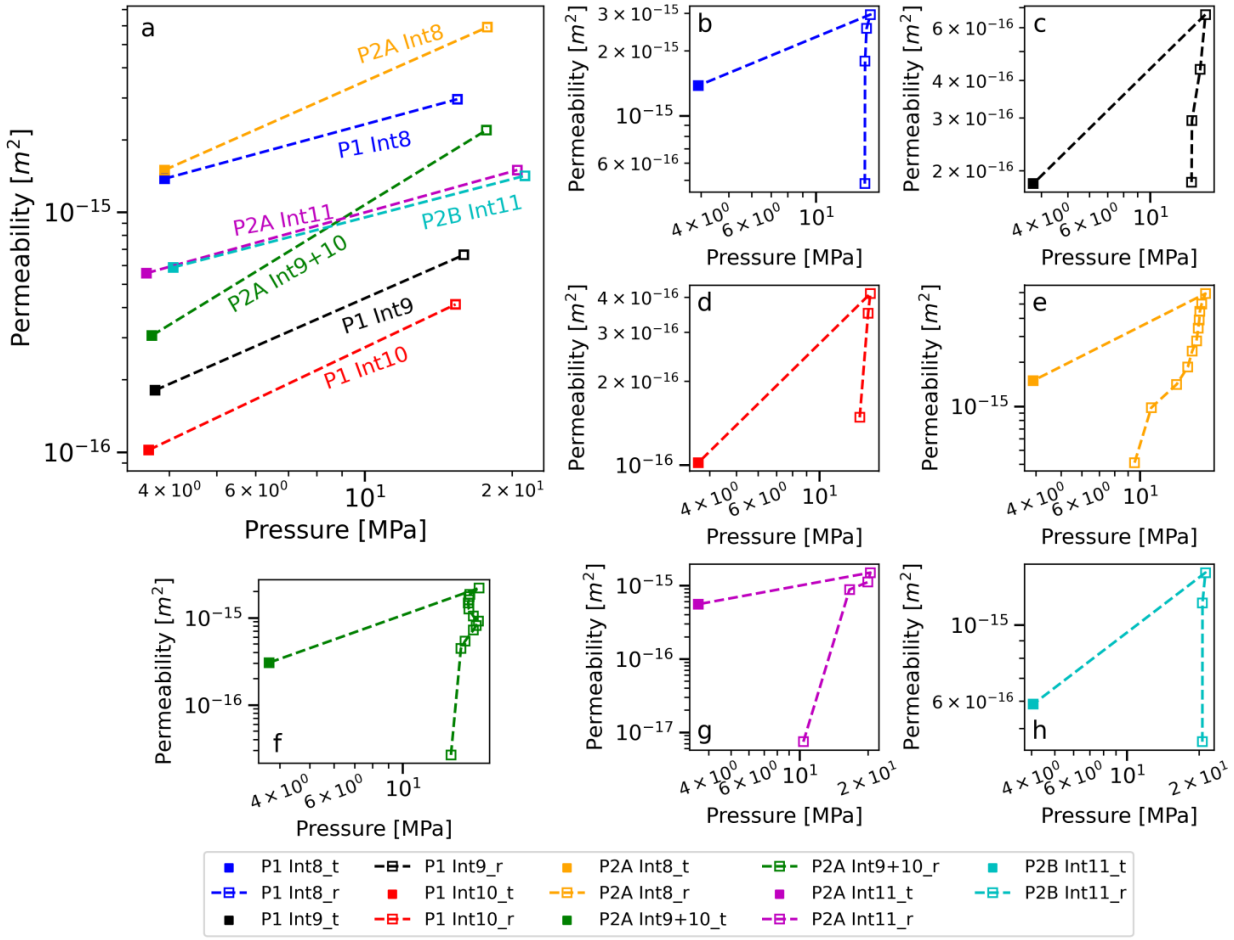

Figure 5. Pressure-dependent permeability evolution and comparison with final permeability estimated from post-stimulation hydrotest transmissivity measurements for all stimulation experiments in Phases 1 and 2. (a) Comparison between peak permeability estimated during stimulation (open squares) and permeability recorded in hydrotests (filled squares). (b–h) Permeability evolution occurs during each stimulation step, where the dashed lines connect points sequentially in time. Yu et al., 2025.

Highlight 3: Scaling Relationships Between Seismic Moment and Permeability Changes During Shear Reactivation: Insights from Laboratory to Field-Scale Observations

We established the physical basis for seismicity–permeability scaling relationships with carefully controlled laboratory experiments and integrating them with field-scale observations (Yu et al., 2025b). Our laboratory tests were performed on preexisting faults in both Westerly granite and Utah FORGE granitoid samples. Under two boundary conditions (zero displacement or constant stress), faults were reactivated through stepwise increases in fluid pressure. At each pressure increment, we measured the induced permeability changes and recorded the cumulative seismic moment (M) of acoustic emission (AE) events, capturing the entire cycle of fracture reactivation. A representative experiment (PL02, Fig. 6) conducted under the zero-displacement boundary condition illustrates the methods. In this test, the upstream pressure was incremented in fixed steps (e.g., by 0.5 MPa) while the downstream pressure was held constant at 0.5 MPa. Permeability was estimated at each step from the flow rate measured at steady-state conditions. Simultaneously, AE events were detected via a long-term average/short-term average (LTA/STA) algorithm. Most events occurred in tandem with each pressure increase and subsequent shear slip. We then computed incremental permeability changes, $\Delta k_i = k_i - k_{i-1}$, and correlated them with binned AE-derived cumulative seismic moments for each pressure step.

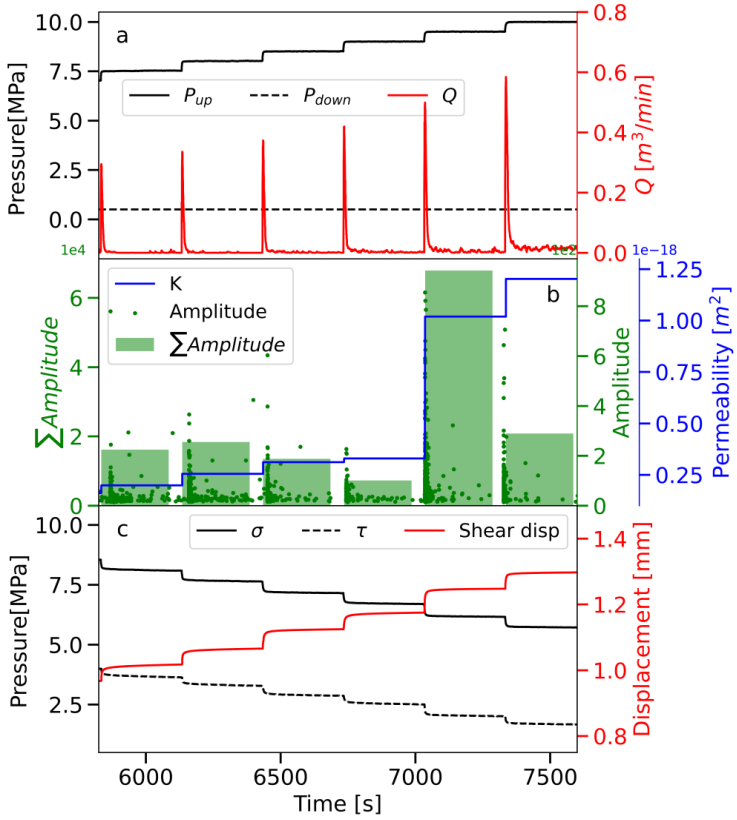

Figure 6: Observed permeability enhancement and cumulative amplitudes of Acoustic Emission (AE) events during each pressure step induced by fluid injection in experiment PL02 under zero-displacement conditions. (a) Prescribed histories of downstream and upstream pressure, and evolving upstream injection rate Q. (b) Induced AE event amplitudes, cumulative amplitude per step, and measured steady-state permeability per step. (c) Effective normal stress, shear stress, and shear displacement changes during the shear reactivation experiment. Yu et al., 2025b

Seismic moments and permeability changes each span an order of magnitude in individual experiments (Fig.7(b-e)) and are broadly linearly proportional (Fig.7(b-e)). Overall this ensemble linear proportionality spans ~3-4 orders of magnitude in seismic moment and permeability and is consistent with previous characterizations inferred from field data. Thus, linear scaling is indeed suggested with $M \propto \Delta k$ across the specific centimeter length scale of this laboratory fault.
We attempt to define a direct quantitative link between change in permeability and seismic moment. Based on the physical relationship between seismic moment and permeability change proposed previously, $\Delta k = M_0 \Delta\tau^2 \alpha^3 / 12 s G^3$, we compare the permeability changes (ΔK_d) calculated using this model with the experimentally measured permeability changes (ΔK_{raw}) in Fig. 8 using the parameters above – showing excellent correspondence. These results indicate an excellent fit of the model, with high R^2 values, validating the linearly proportional relationship of $\Delta k = \omega M_0$ at centimeter-scale within the laboratory experiments.

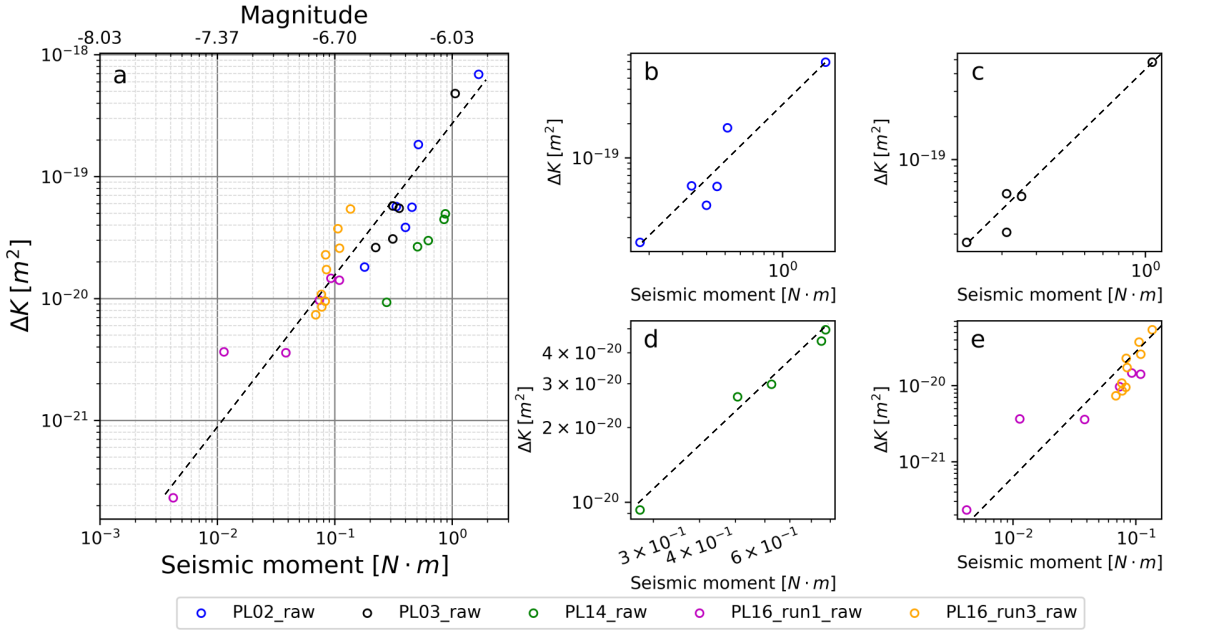

Figure 7: Cumulative seismic moment versus calculated permeability changes for five shear reactivation experiments. (a) Combined data for all five experiments, showing cumulative seismic moment versus permeability changes in each pressure step. (b), (c), (d), and (e). Individual plots for each experiment, depicting the relationship between cumulative seismic moment and permeability changes for each pressure step. Dashed lines represent best fit through laboratory data. Yu et al., 2025b

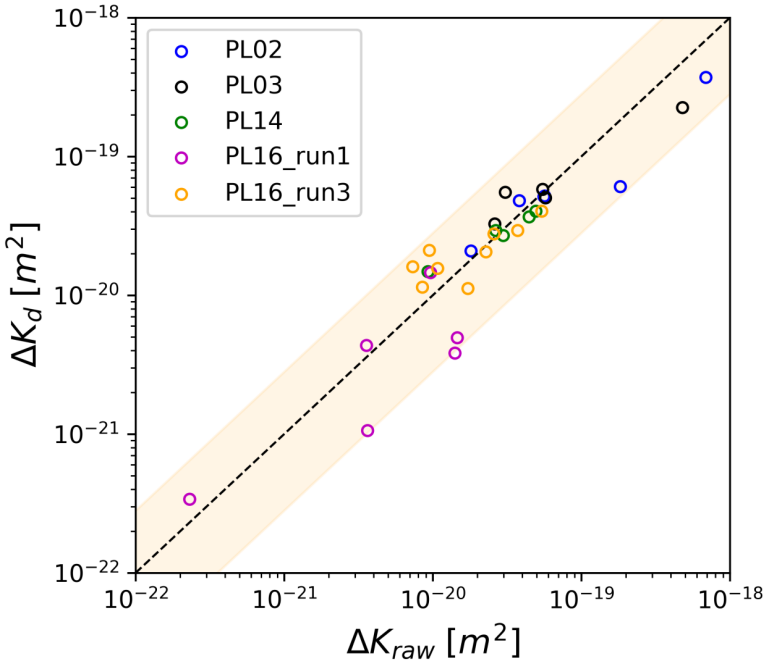

Figure 8: Comparison between permeability changes observed in experiments and those calculated based on the proposed model for all shear reactivation experiments. ΔK_{raw} represent the permeability changes evaluated from the steady-state period of each pressure step, with ΔK_d the permeability changes calculated from laboratory measured seismic moment and stress drop based on the proposed linear relationship. (Yu et al., 2025b)

Extending these findings to the field, where larger-scale data incorporate multiple fault segments and heterogeneous stress conditions, we observe that Δk aligns more comprehensively with $\Delta k \propto M_0^{2/3}$. This scaling function accommodates the influence of broader fracture networks and variable stress drops—factors that become increasingly significant over kilometer-scale domains. The refined relationship not only reconciles laboratory and field datasets but also highlights the potential for using microearthquake records to infer evolving permeability in crustal reservoirs.

These insights build upon previous studies linking crustal permeability changes to cumulative seismic moment. By integrating well-constrained laboratory experiments, physically based modeling, and multi-scale field observations, we strengthen the mechanistic understanding of how shear-induced displacements modulate fracture apertures and thus permeability. Importantly, the evolving power law relationship provides a robust framework for predicting permeability evolution in low-permeability rocks subjected to hydraulic stimulations. The results of this research are currently under second-round review (Yu et al., 2025b).

Highlight 4: ML models for predicting seismicity and magnitude rate from injection features

We developed a novel hybrid machine learning framework to predict seismicity rates and magnitude rates (expressed as the number of MEQ events or the average logarithmic seismic moment within a given time window) using injection parameters from the 2022 Utah FORGE geothermal hydraulic stimulations. Key input features include injection rate, temporal gradients in pressure (dp/dt), radial variations in pressure (dp/dr), and injection distance R.

Our approach combines a Bayesian Long Short-Term Memory (LSTM) model with a Multi-Head Attention mechanism to capture temporal dependencies in sequential data and to quantify uncertainty. By employing variational inference, the Bayesian LSTM delivers probabilistic outputs with confidence intervals. The Bayesian LSTM's predictions—mean and uncertainty bounds—were then integrated with the original features and fed into an XGBoost regressor, leveraging the sequential modeling strengths of the Bayesian LSTM and the robust feature-handling capabilities of XGBoost. This two-stage model was trained and validated on three sequential stages of the 2022 Utah FORGE hydraulic stimulation of Well 16A. Stage 1 served as the training dataset, Stage 2 as validation, and Stage 3 as the testing dataset. The hybrid framework effectively predicted both seismicity rates (Fig. 9) and magnitude rates (Fig. 10) in the validation and testing phases, offering accurate predictions along with credible intervals. Such predictive capability is vital for risk assessment and mitigation in geothermal operations, as it informs operators about the likelihood of induced seismic events.

In parallel, we derived a physics-based relationship that links seismic moment (and thus magnitude) to key operational injection parameters. Among the variables analyzed, three dominant parameters emerged as primary controls on MEQ magnitude.

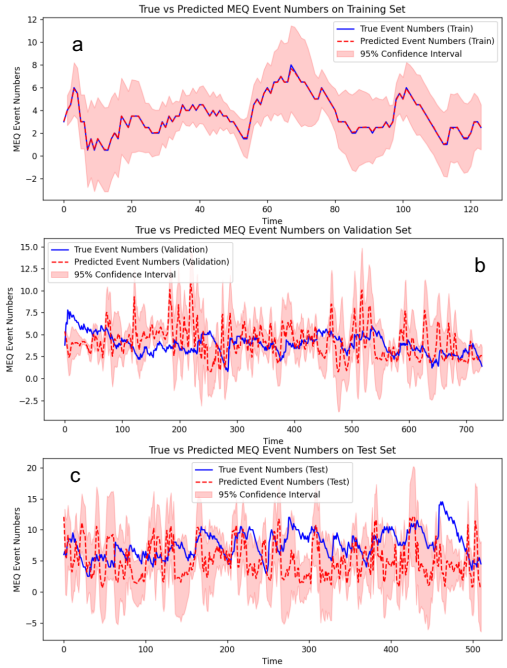

Figure 9: model seismicity rate prediction results compared with groud truth by using FORGE stage 1 as train dataset (a), FORGE stage 2 as validation dataset (b) and FORGE stage 3 as test dataset (c).

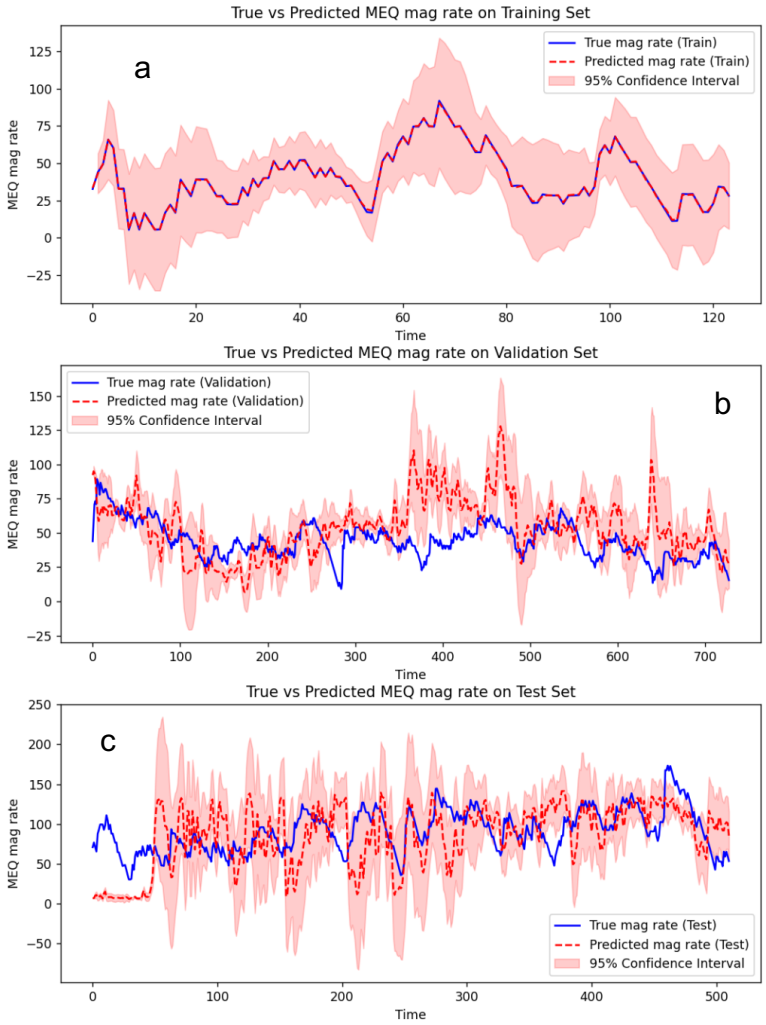

Figure 10: model magnitude rate prediction results compared with groud truth by using FORGE stage 1 as train dataset (a), FORGE stage 2 as validation dataset (b) and FORGE stage 3 as test dataset (c).

Highlight 5: DASEventNet—A Deep Learning Model for MEQ Detection in DAS Data

In this study, we developed a deep learning architecture, termed DASEventNet, to detect microearthquakes (MEQs) in continuous distributed acoustic sensing (DAS) data acquired during the April 2022 hydraulic stimulations at Utah FORGE Well 16A (78)-32. The training dataset, which comprised 1,292 cataloged MEQs and an equivalent number of noise samples from Well 78B-32, enabled the model to achieve a perfect 100% accuracy on a test set of 260 samples. To gain insights into the model's internal decision-making process, we visualized activation maps for both MEQ and noise segments. These maps revealed high activation values corresponding to MEQ signals and lower or negative activations in regions classified as noise (Fig. 11), underscoring that the learned features align with expert assessments.

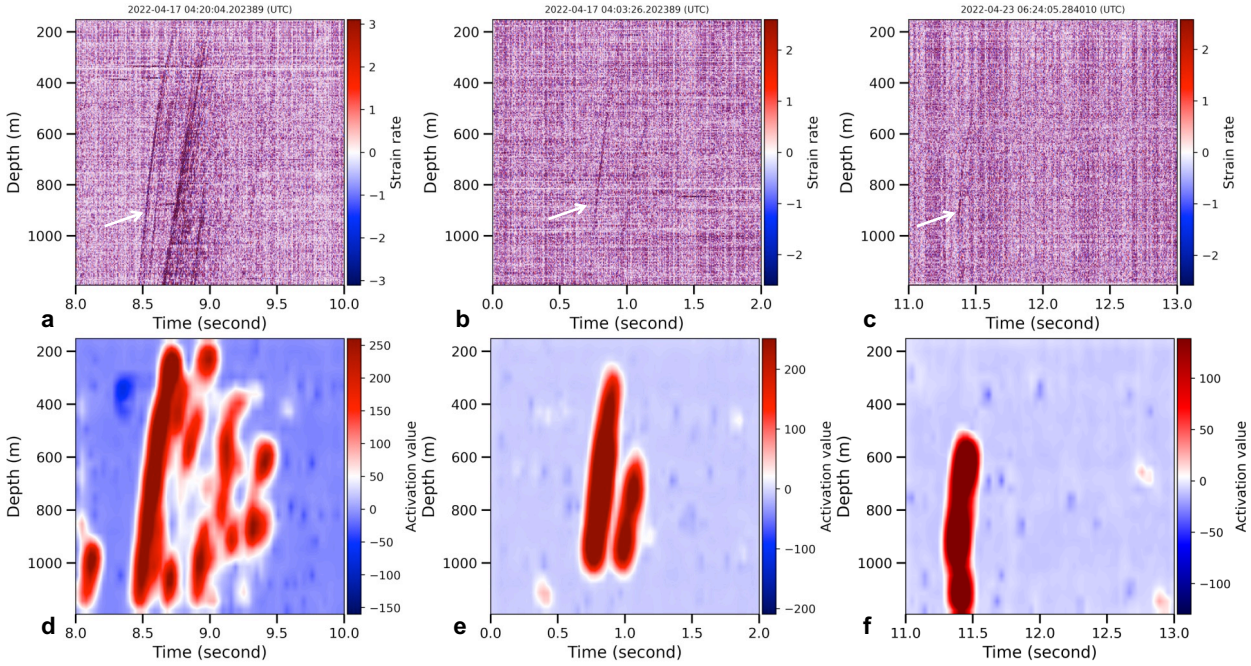

Figure 11: Comparative visualization of original event inputs and CAMs for the DASEventNet model. Panels (a-c) display three examples of input events processed by the model. Panels (d-f) correspond to their respective CAM, which illuminate the regions within the inputs that are most influential in guiding the model classification decisions. Yu et al., 2024b.

Notably, DASEventNet demonstrated the capacity to detect weak MEQs initially labeled as noise (Fig. 12) and to accurately delineate the event signal within tube-wave noise (Fig. 13). Upon application to the entire DAS dataset throughout the stimulation period, DASEventNet identified 7,058 MEQs—significantly exceeding the 1,309 events detected by the standard STA/LTA method. This fivefold increase includes newly detected events with magnitudes as low as $Mw - M_w - 1.80$, whereas STA/LTA methods were limited to $M_w - 1.14$ (Fig. 14).

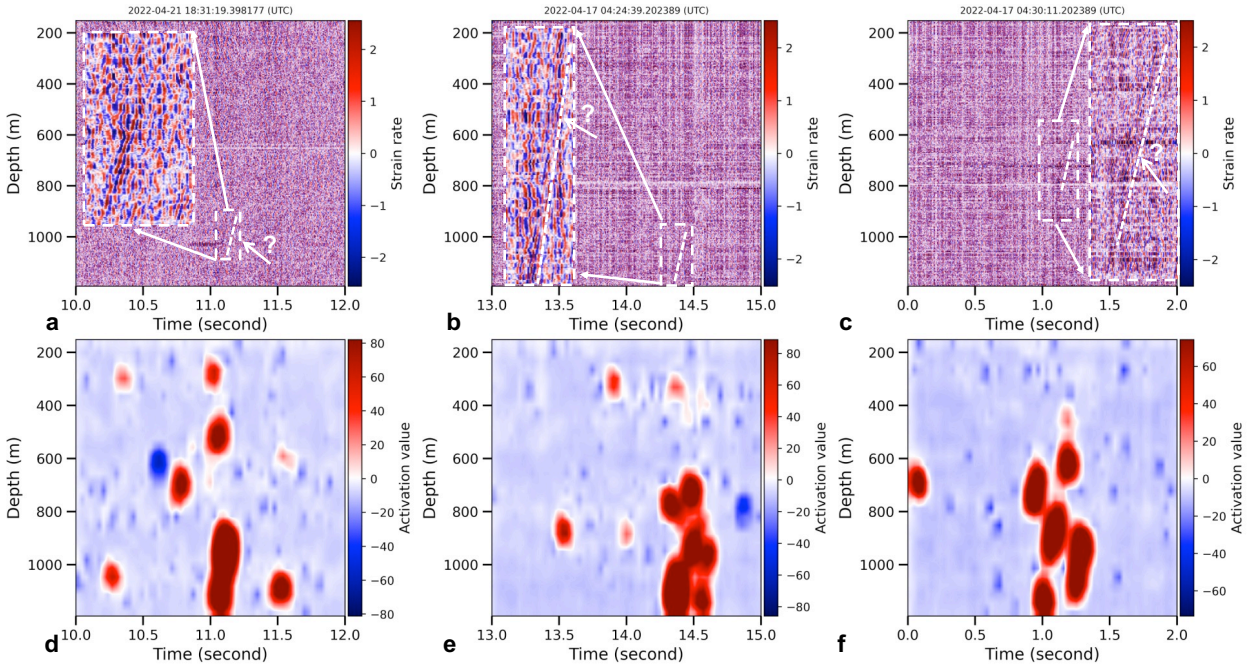

Figure 12: Comparative visualization of original inputs and their CAMs for the DASEventNet model. Panels (a-c) display three examples of inputs where event signals are not visually apparent. Panels (c-d) correspond to their respective CAMs with highlighted weak event signal regions. The weak event signals are zoomed in and shown within the white frames for better visualization. Yu et al., 2024b

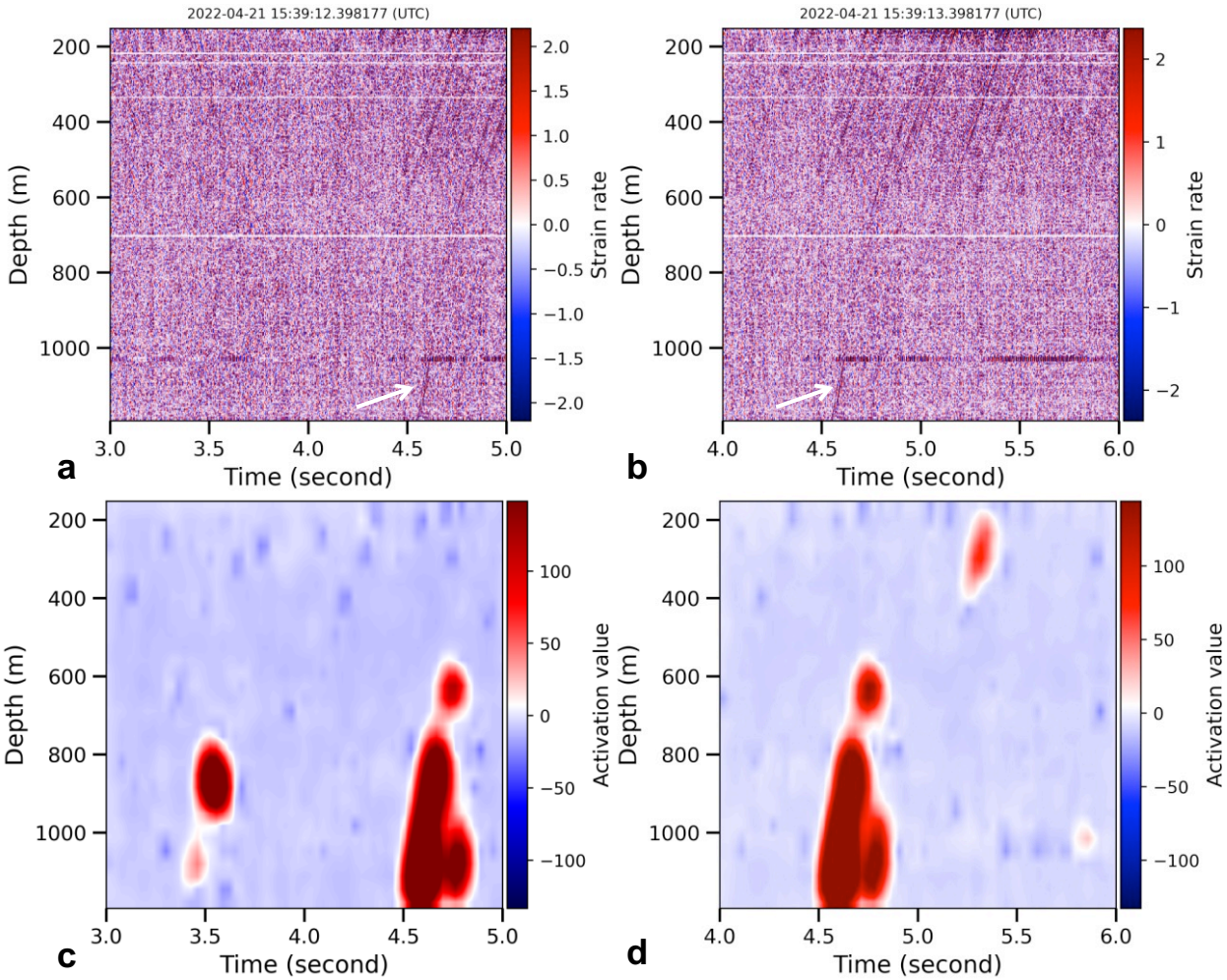

Figure 13: Data examples including both tube-wave noise and event signals (a-b), and their CAMs(c-d) for the DASEventNet model. Yu et al., 2024b

Enhanced by this expanded catalog, we observed that seismicity rates correlate strongly with injectivity evolution in Stage 3 of the stimulations, suggesting evolving permeability. Moreover, the spatial distribution of these MEQs indicates the successful creation of a stimulated reservoir volume via reactivated fracture networks. These results are particularly noteworthy given the partial limitations of fiber placement in Well 78B-32. Overall, the high sensitivity and reliability of DASEventNet afford unprecedented clarity on how fractures respond to stimulation, thereby improving seismic hazard assessment and reservoir characterization. Additionally, DASEventNet's applicability extends to real-time or long-term surveillance, including monitoring production-induced seismicity caused by cold-water injections in Enhanced Geothermal System (EGS) operations. The details of this work have been published in *JGR: Solid Earth* (Yu et al., 2024b).

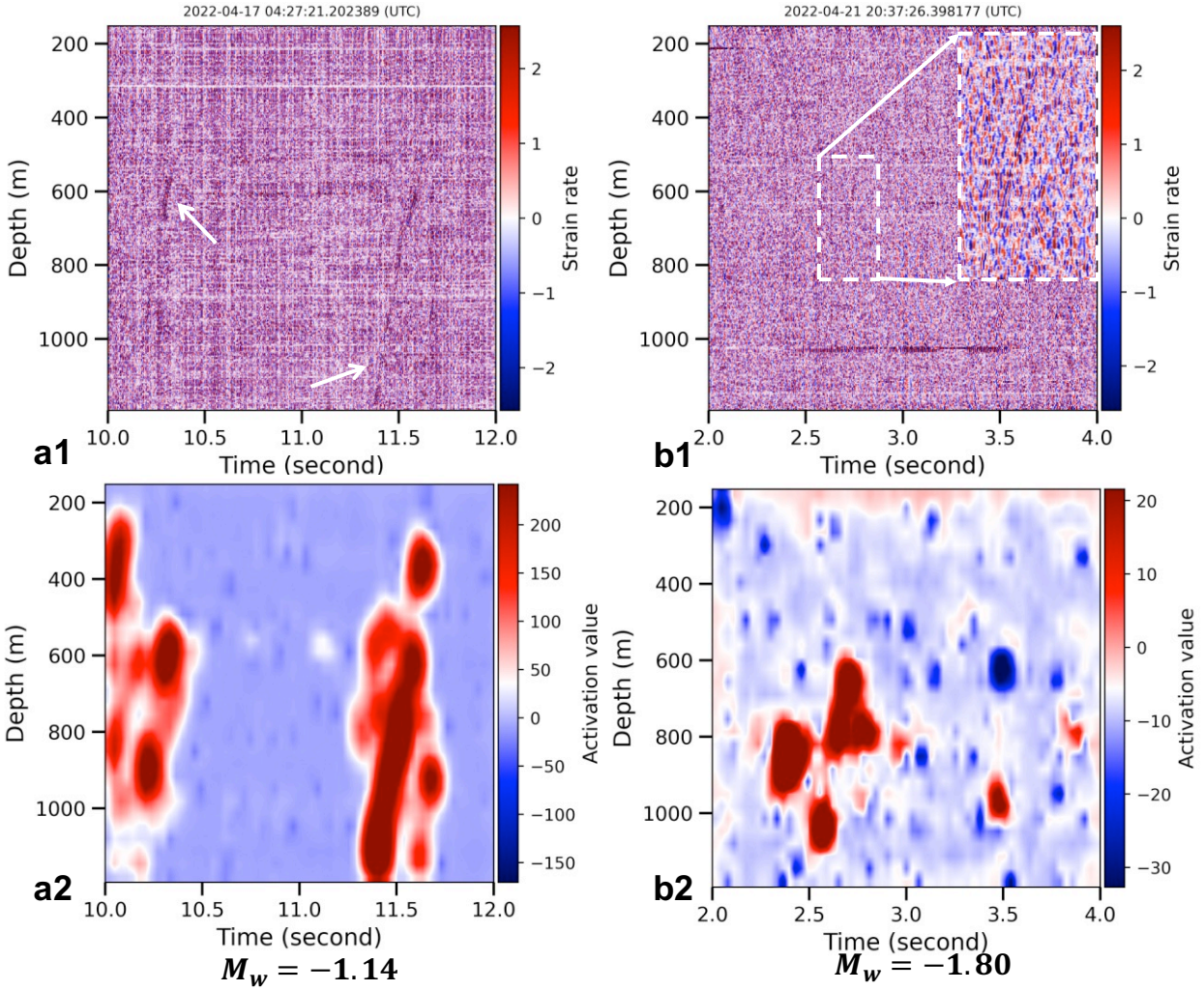

Figure 14: Comparison of minimum magnitude between events detected by the DASEventNet model and the STA/LTA Method. Panel (a1) shows the original DAS records with a magnitude of -1.14, the minimum event magnitude detectable by the STA/LTA method. Panel (b1) shows the original DAS records with a magnitude of -1.80, detectable solely by the proposed DASEventNet model. Panels (a2, b2) present the corresponding CAM plots for (a1) and (b1), respectively. The weak event signals are zoomed in and shown within the white frames for better visualization. Yu et al., 2024b

Highlight 6: DASEventLocNet—A Physics-Informed Transformer for MEQ Localization with DAS Data

In this work, we developed a physics-informed Transformer model, DASEventLocNet, to locate microseismic events (MEQs) induced by hydraulic stimulation at Utah FORGE Well 16A (78)-32. Employing the Utah FORGE velocity model for forward waveform modeling, we generated synthetic Distributed Acoustic Sensing (DAS) data that included noise, coherent S-wave signals, and masked channels to emulate real-world DAS recordings. DASEventLocNet directly ingests DAS waveforms (spanning 2D windows of 300 channels by 1 second) and outputs the three-dimensional (X, Y, Z) coordinates of MEQ hypocenters. Figs 15 and 16 illustrate the model's robust performance on validation and test sets, with most events localized within 100–200 meters of their true locations. Despite simulated interference (e.g., masked channels, strong random noise, incoherent S-wave signals), 95% of predicted event locations deviated by under 100 meters from the ground-truth coordinates, underscoring the model's resilience to data corruption.

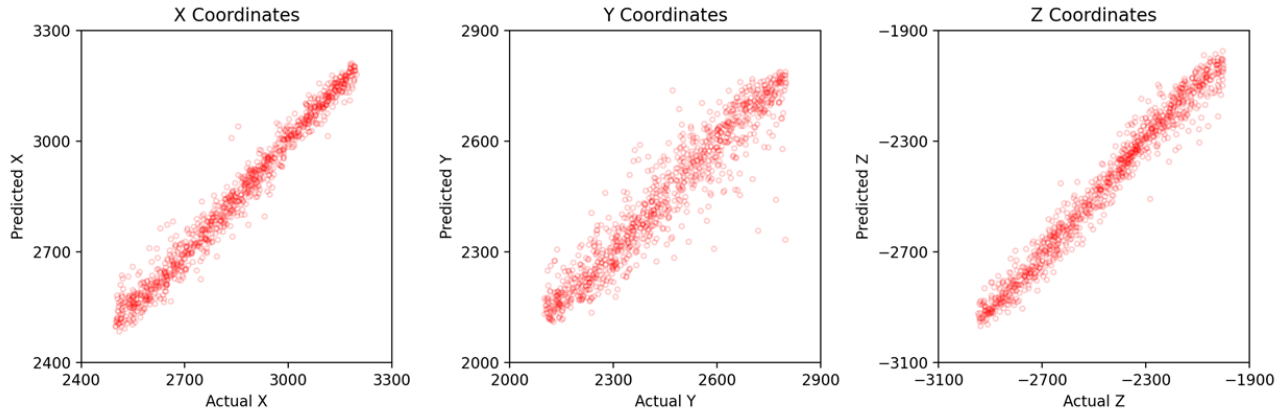

Figure 15: Comparison of predicted and actual event locations in the validation dataset including 1000 MEQs

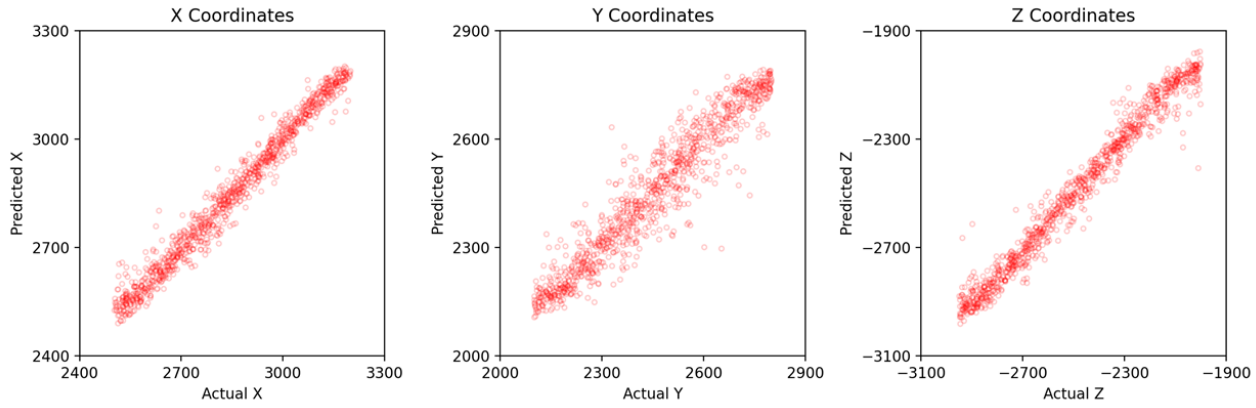

Figure 16: Comparison of predicted and actual event locations in the **unseen test** dataset including 1000 MEQs

We analyzed the prediction errors by comparing the predicted locations with the true event locations. As illustrated in Figure 17, the model predicted the locations of 95% of MEQs with an

error smaller than 100 meters in both the validation and test datasets. Moreover, 97% of the predicted MEQ locations had errors smaller than 200 meters. Considering the substantial noise we introduced into the data, these results are considerably good.

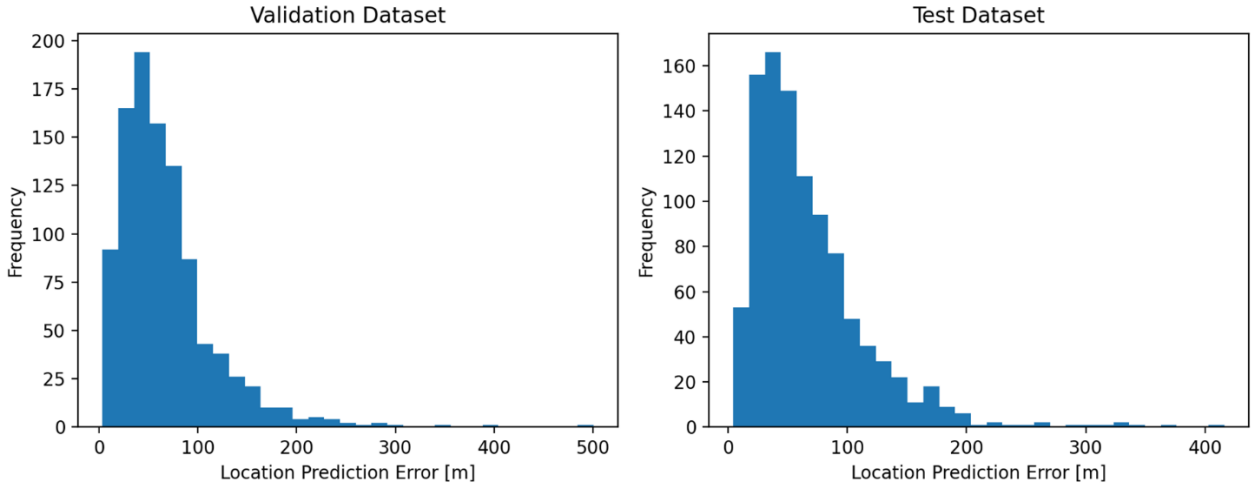

Figure 17: Model location error on validation(1000MEQs) and test dataset (1000 MEQs), the location error is calculated by $D_{error} = \sqrt{(x_p - x_t)^2 + (y_p - y_t)^2 + (z_p - z_t)^2}$, where x_p, y_p, z_p are the predicted coordinates of a MEQ by the model, x_t, y_t, z_t are the true coordinates of a MEQ.

We subsequently applied DASEventLocNet to a set of 1,200 MEQ signals recorded by DAS fiber in Utah FORGE Well 78B-32. Location errors in this real dataset averaged 120 meters (±36 meters, Fig. 18), a result only moderately larger than the ~70-meter average error observed in synthetic data. Crucially, the model preserved its localization accuracy even though the 78B fiber is situated at a shallower depth (1,500–1,800 m from the stimulation zone) compared to deeper geophone boreholes. When compared with two existing catalogs—(1) the Silixa DAS-based catalog (78A and 78B fibers) and (2) the deep geophone borehole catalog, the developed DASEventLocNet consistently generated MEQ clusters closely matching those from the more reliable deep borehole geophones (Fig.19). By contrast, the Silixa catalog's MEQ locations appeared sparser and more scattered, signifying larger errors (Fig.19). This result indicates that DASEventLocNet significantly refines MEQ locations using only a single vertical DAS fiber, resolving potential challenges in horizontal (X and Y) resolution.

Overall, DASEventLocNet offers a physics-grounded, Transformer-based framework for robust and accurate microseismic event localization, even under noise-ridden and limited-angle recording conditions. Its capabilities hold promise for real-time seismic monitoring and reservoir characterization in enhanced geothermal systems (EGS) and other subsurface applications. These findings will form the basis of an upcoming manuscript currently in preparation.

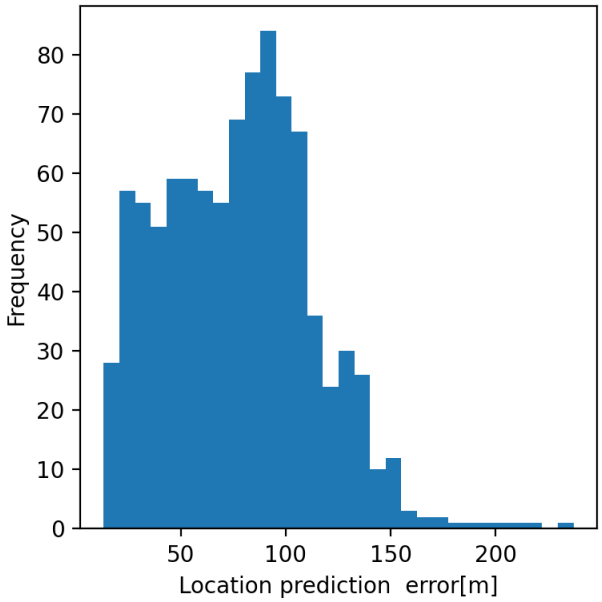

Figure 18: Prediction errors in MEQ locations of DASEventLocNet model for 1,200 real events, derived from 78B Distributed Acoustic Sensing (DAS) fiber recordings during the 2022 FORGE hydraulic stimulations. The location error is calculated by $D_{error} = \sqrt{(x_p - x_t)^2 + (y_p - y_t)^2 + (z_p - z_t)^2}$, where x_p, y_p, z_p are the predicted coordinates of a MEQ by the model, x_t, y_t, z_t are the true coordinates of a MEQ.

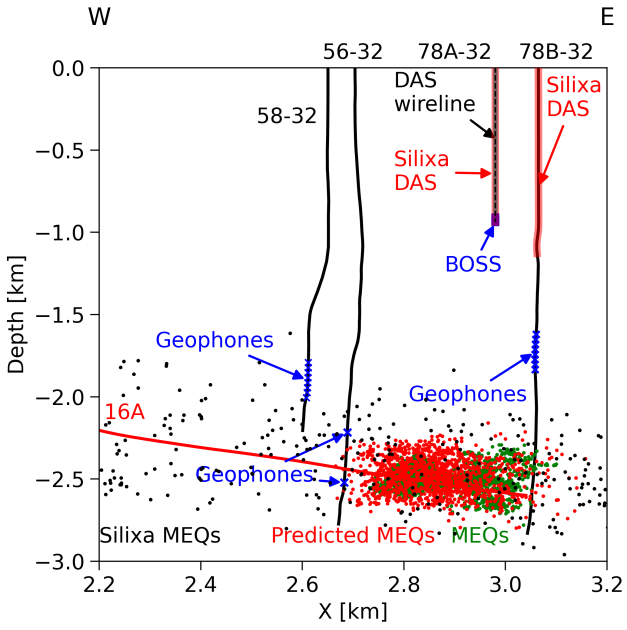

Figure 19: Comparison of MEQ location predictions across three catalogs: the Silixa catalog (black), the deep borehole geophone catalog (green), and the DASEventLocNet catalog (red).

Highlight 7: Acoustic energy release during the laboratory seismic cycle: Insights on laboratory earthquake precursors and prediction.

This work demonstrates that machine learning can predict the timing and magnitude of laboratory earthquakes using statistics of acoustic emissions. We showed that the evolution of acoustic energy is critical for lab earthquake prediction; however, the connections between acoustic energy and fault zone processes leading to failure remain poorly understood. Here, we documented in detail the temporal evolution of acoustic energy during the laboratory seismic cycle. We conducted friction experiments for a range of shearing velocities, normal stresses, and granular particle sizes. Acoustic emission data were recorded continuously throughout shear using broadband piezoceramic sensors. We found that the coseismic acoustic energy release scales directly with stress drop and is consistent with concepts of frictional contact mechanics and time - dependent fault healing (Figure 20). Experiments conducted with larger grains show that the temporal evolution of acoustic energy scales directly with fault slip rate. In particular, the acoustic energy is low when the fault is locked and increases to a maximum during coseismic failure (Figure 21). Data from traditional slide-hold-slide friction tests confirm that acoustic energy release is closely linked to fault slip rate. Furthermore, variations in the true contact area of fault zone particles play a key role in the generation of acoustic energy. Our data show that acoustic radiation is related primarily to breaking/sliding of frictional contact junctions, which suggests that machine learning - based laboratory earthquake prediction derives from frictional weakening processes that begin very early in the seismic cycle and well before macroscopic failure.

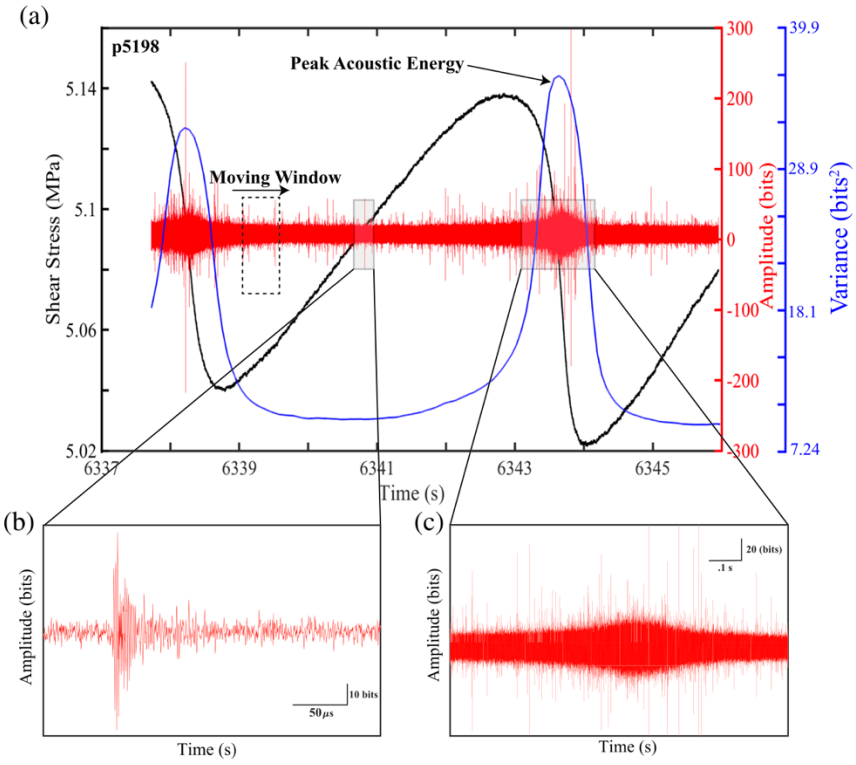

Figure 20: (a) Shear stress, acoustic amplitude, and acoustic variance plotted as a function of time for one seismic cycle. The dashed rectangle shows our moving window (0.636 s) used to compute the acoustic variance. At this scale acoustic data look like noise; however, the signal is composed of individual AEs

(some identifiable as small spikes) that grow in size and number as failure approaches (see b). The acoustic variance first decays following a failure event, reaches a minimum during the interseismic period, and finally begins to increase prior to failure. (b) Zoom of an AE that nucleated during the interseismic period. (c) Zoom of the acoustic signal during coseismic failure. Note the broad, low amplitude nature of the envelope with superimposed high - frequency AEs. (Bolton et al., 2020).

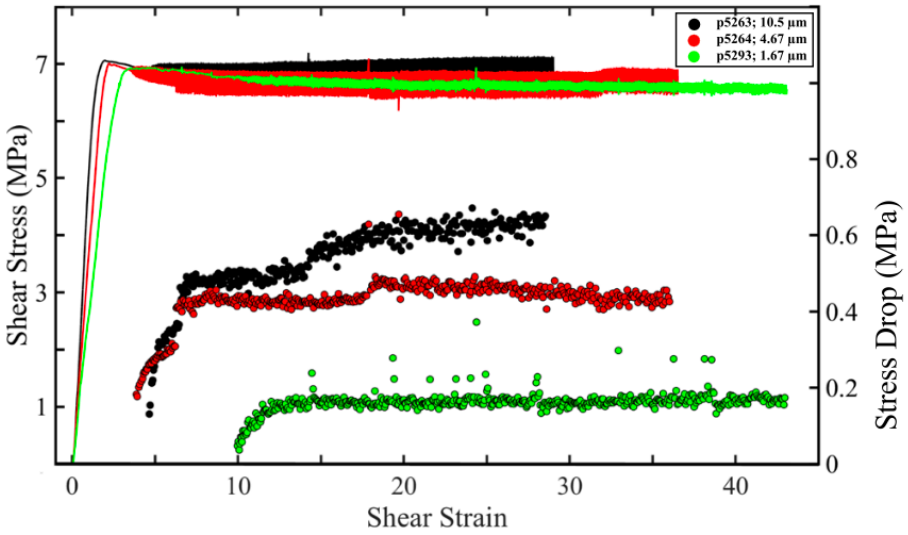

Figure 21: Shear stress and stress drop as a function of shear strain for experiments conducted with different median grain sizes. Note that stress drop increases during the initial part of each experiment and reaches a steady state for which larger grains produce bigger events. (Bolton et al., 2020).

Highlight 8: Predicting lab earthquakes using physics-informed neural networks and fault zone acoustic monitoring

This work demonstrates powerful new techniques for predicting failure in solids (Borat et al., 2023). We build on recent machine learning work showing that laboratory earthquakes can be predicted using micro-failure events and temporal evolution of fault zone elastic properties. Remarkably, these results come from purely data-driven models trained with large datasets. Such data are equivalent to centuries of fault motion rendering application to tectonic faulting unclear. In addition, the underlying physics of such predictions is poorly understood. Here, we address scalability using a novel Physics- Informed Neural Network (PINN). Our model encodes fault physics in the deep learning loss function using time-lapse ultrasonic data. PINN models outperform data-driven models and significantly improve transfer learning for small training datasets and conditions outside those used in training.

We developed new techniques for feature extraction process (Figure 22). Physics-based features, namely wave speed (vi) and spectral amplitude (Ai) at time ti, are extracted from each ultrasonic signal waveform. To calculate the evolution of wave speed during frictional sliding, we first extract the time delay Δt by cross-correlating each waveform Si with a reference waveform S0. The reference waveform is chosen past the peak friction just before the fault starts its transition from stable sliding to unstable seismic cycles (thin vertical dashed line at time = 2065 s in Fig. 1a). The shape of the recorded waveforms Si changes little throughout the experiment. Our work suggests that PINN offers a promising path for machine learning-based failure prediction and, ultimately for improving our understanding of earthquake physics and prediction.

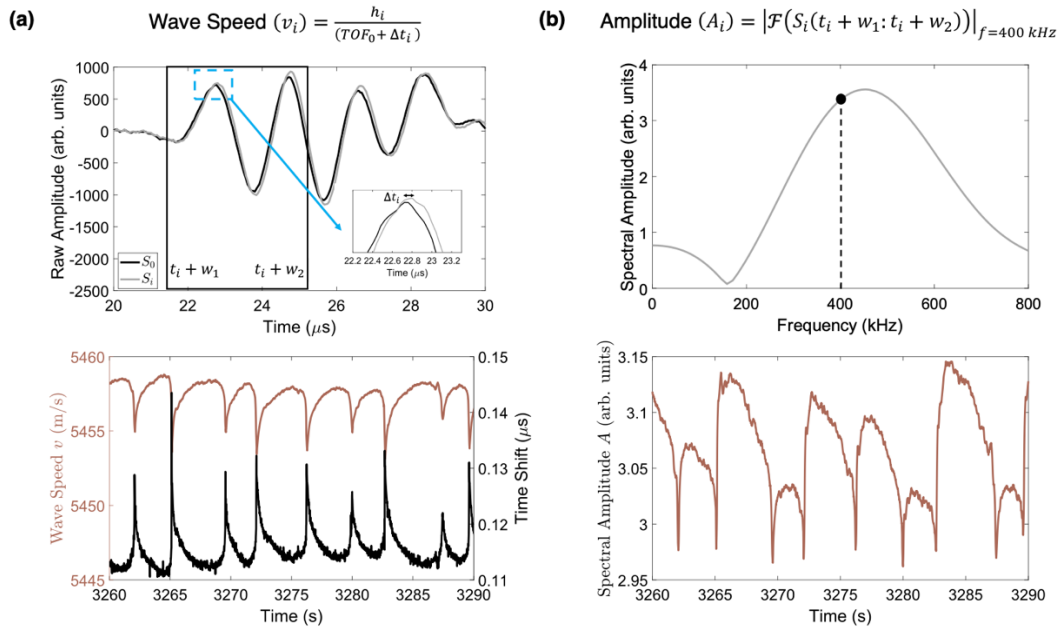

Figure 22: Details of the feature extraction procedure. (a) Shows the reference waveform (S0) and a typical waveform during shearing (Si). The inset emphasizes the time delay between the two signals Δti calculated by cross-correlating the two signals. The box marks the extent of the cross-correlation window from ti + w1 to ti + w2 with w1 = 20.76 μs and w2 = 25.16 μs. The bottom plot shows a sample of wave speed and time shift evolution for several lab seismic cycles over a period of 30 s. (Borat et al., 2023).

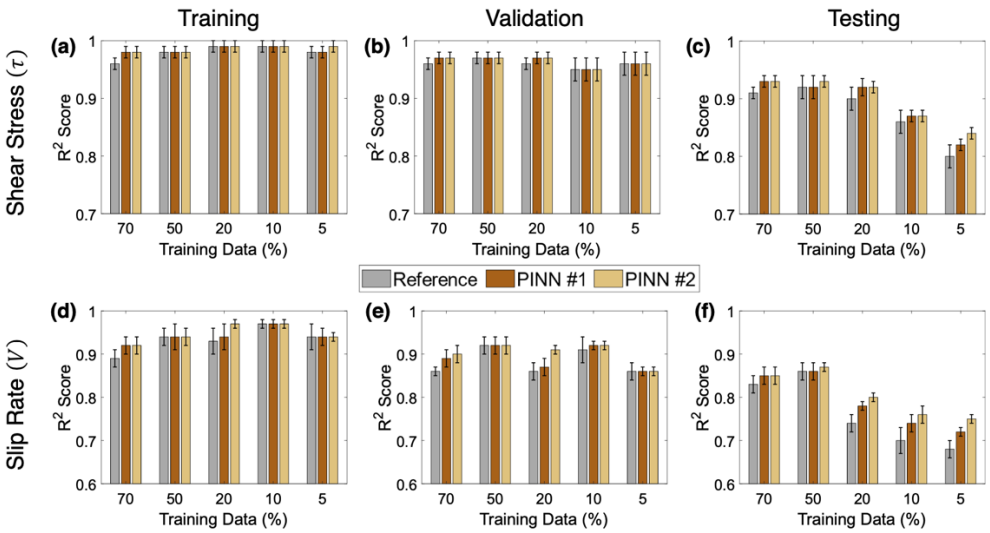

Figure 23: Performance of the Reference data-driven, PINN #1, and PINN #2 models for experiment p5270. a–c Shear stress (τ) prediction R2 scores in training, validation, and testing as a function of varying training set sizes. d–f Slip rate (V) prediction R2 scores in training, validation, and testing datasets as a function of varying training set sizes are plotted. For both shear stress and slip rate, the PINN models outperform the reference data-driven models in testing and the improvement increases inversely with training data size. The minimum and maximum of the error bar represent the one standard error from the mean. (Borat et al., 2023).

8 Significant Accomplishments and Conclusions

Our work has produced a transformational advance in our understanding of reservoir imaging, induced seismicity, and earthquake prediction. Our methods have made it possible to image and track fluid plumes in underground reservoirs. Those observations have been used to illuminate the nonlinear relationship between fluid flow, seismic wave speed, and non-linear elasticity.

The project has many products and many significant accomplishments and conclusions. Section 7 contains an executive summary of seven products and Section 10 contains the full references for each of the 32 products that came from this work. In addition to the 32 publications the project supported the work of 6 PhD students, 40 conference presentations, 6 keynote talks at national meetings, and mentoring and professional development for 4 postdoctoral fellows

9. Path Forward

Given the progress that was made by this project in a short time frame of just a few years there are many directions for future work. Chief among these are further efforts to apply lab-based ML methods to identify precursors to failure and monitor fault zone stress state during the seismic cycle to field settings and reservoir conditions. If DOE Geothermal decides to support further work in these areas we will be happy to help with those goals.

10. Products

All accepted manuscripts have been uploaded to OSTI

1. Affinito, R., Wood, C. Marty, S., Elsworth, D. and C. Marone, The stability transition from stable to unstable frictional slip with finite pore pressure, *Geophys. Res. Lett.*, 51, doi. org/10.1029/2023GL105568, 2024.
2. An, M., Zhang, F., Yin, Z., Huang, R., Elsworth, D. and C. Marone, Frictional strength and frictional instability of glaucophane gouges at blueschist temperatures support diverse modes of fault slip from slow slip events to moderate-sized earthquakes, *J. Geophys. Res.*, 129, doi.org/10.1029/2023JB028399, 2024.
3. Bolton, D. C., Marone, C., Saffer, D. M., and D. T. Trugman, Foreshock properties illuminate nucleation processes of slow and fast laboratory earthquakes, *Nat. Comm.*, *14:3859*, doi.org/10.1038/s41467-023-39399-0, 2023.
4. Bolton, D. C., Shreedharan, S., McLaskey, G. C., Rivière, J., Shokouhi, P., Trugman, D. T. and C. Marone, The high-frequency signature of slow and fast laboratory earthquakes, *J. Geophys. Res. Solid Earth*, 127, *doi.org/10.1029/2022JB024170*, 2022.
5. Bolton, D. C., Shreedharan, S., Rivière, J., and C. Marone, Frequency-magnitude statistics of laboratory foreshocks vary with shear velocity, fault slip rate, and shear stress, *J. Geophys. Res. Solid Earth*, 126, 10.1029/2021JB022175, 2021.
6. Bolton, D. C., Shreedharan, S., Rivière, J., and C. Marone, Acoustic energy release during the laboratory seismic cycle: Insights on laboratory earthquake precursors and prediction. *J. Geophys. Res. Solid Earth*, *125*, 10.1029/2019JB018975, 2020.
7. Borat, P. Rivière, J., Marone, C., Mali, A, Kifer, D. and P. Shokouhi, Using a physics-informed neural network and fault zone acoustic monitoring to predict lab earthquakes, *Nat. Comm.*, *14:3693*, doi.org/10.1038/s41467-023-39377-6, 2023.
8. Borate, P. Rivière, J., Marty, S., Marone, C., Kifer, D. and P. Shokouhi, Physics informed neural network can retrieve rate and state friction parameters from acoustic monitoring of laboratory stick-slip experiments, *Scientific Reports*, 14:24624, doi.org/10.1038/s41598-024-75826-y, 2024.
9. Cebry, S. B. L., Ke, C. Y., Shreedharan, S., Marone, C., Kammer, D. S., and G. C. McLaskey, Creep fronts and complexity in laboratory earthquake sequences illuminate delayed earthquake triggering, *Nat. Comm.*, 13:6839, doi.org/10.1038/s41467-022-34397-0, 2022.
10. Chiaraluce, L., Bennett, R., Mencin, D., Johnson, W., Barchi, M, Bohnhoff, M., Baccheschi, P., Caracausi, A., Calamita, C., Cavaliere, A., Gualandi, A., Mandler, E., Mariucci, M.T., Martelli, L., Marzorati, S., Montone, P., Pantaleo, D, Pucci, S., Serpelloni, E., Supino, M., Stramondo, S., Hanagan, C. Van Boskirk, L., Gottlieb, M., Mattioli. G., Urbani, M. Mirabella F., Akimbekova, A., Pierdominici, S., Wiersberg, T., Marone, C. Palmieri, L. and L. Schenato, A strainmeter array as the fulcrum of novel observatory sites along the Alto Tiberina Near Fault Observatory, *Sci. Dril.*, 33, 173–190, doi.org/10.5194/sd-33-173-2024, 2024.

11. den Hartog, S. A. M., Marone, C. and D. M. Saffer, Frictional behavior downdip along the subduction megathrust: insights from laboratory experiments on exhumed samples at in-situ conditions, *J. Geophys. Res. Solid Earth*, 128, *doi.org/10.1029/2022JB024435*, 2023.
12. Guyer, R. A., Marty, S. Johnson, C. W., Johnson, P. A., and C. Marone, On the anatomy of acoustic emission, *J. Acoust. Soc. Am.*, 156, 4116–4122, 2024.
13. Jaspereson, H., Bolton, D. C., Johnson, P. A., Guyer, R., Marone, C. and M. V. de Hoop, Attention network forecasts time-to-failure in laboratory shear experiments, *J. Geophys. Res. Solid Earth*, 126, 10.1029/2021JB022195, 2021.
14. Laurenti, L., Paoletti, G., Tinti, E., Galasso, F., Collettini, C., and C. Marone, Probing the evolution of fault properties during the seismic cycle with deep learning, *Nat. Comm.*, doi.org/10.1038/s41467-024-54153-w, 2024
15. Laurenti, L., Tinti, E., Galasso, F., Franco, L., and C. Marone, Deep learning for laboratory earthquake prediction and autoregressive forecasting of fault zone stress, *Earth and Plan. Sci. Lett., 598, 117825, doi.org/10.1016/j.epsl.2022.117825,* 2022.
16. Leong, Z. X., & Zhu, T., Machine learning‐assisted microearthquake location workflow for monitoring the Newberry enhanced geothermal system. Journal of Geophysical Research: Machine Learning and Computation, 1(3), e2024JH000159, 2024a.
17. Leong, Z. X., Zhu, T., & Sun, A. Y., Time-lapse seismic inversion for CO2 saturation with SeisCO2Net: An application to Frio-II site. International Journal of Greenhouse Gas Control, 132, 104058, 2024b.
18. Li, Z., Elsworth, D., Wang, C., & EGS-Collab. (2022). Induced microearthquakes predict permeability creation in the brittle crust. Frontiers in Earth Science, 10, 1020294.
19. Noël, C., Giorgetti, C., Collettini, C., and C. Marone, The effect of shear strain and shear localization on fault healing, *Geophys. J. Int., 10.1093/gji/ggad486,* 2024.
20. Pignalberi, F., Giorgetti, C., Noël, C., Marone, C., Collettini, C., and M. M. Scuderi, The effect of normal stress oscillations on fault slip behavior near the stability tra:nsition from stable to unstable motion, *J. Geophys. Res. Solid Earth*, 129. *doi.org/10.1029/2023JB027470*, 2024.
21. Seyler, C., E., Shreedharan, S., Saffer, D. M., and C. Marone, The role of clay in limiting frictional healing in fault gouges, *Geophys. Res. Lett., 50, doi.org/10.1029/2023GL104984,* 2023.
22. Shreedharan, S., Ikari, M., Wood, C., Saffer, D., Wallace L. and C. Marone Frictional and lithological controls on shallow slow slip at the northern hikurangi margin, *Geochem. Geophys. Geosyst.*, *doi.org*/10.1029/2021GC0101072022, 2022.
23. Shreedharan, S., Bolton, D. C., Rivière, J., and C. Marone, Competition between preslip and deviatoric stress modulates precursors for laboratory earthquakes, *Earth and Plan. Sci. Lett., 553*, 10.1016/j.epsl.2020.116623, 2021.
24. Shreedharan, S., Bolton, D. C., Rivière, J., and C. Marone, Machine learning predicts the timing and shear stress evolution of lab earthquakes using active seismic monitoring of fault zone processes, *J. Geophys. Res. Solid Earth*, 126, 10.1029/2020JB021588, 2021.

25. Wood, C. E., Manogharan, P., Rathbun, A., Rivière, J., Elsworth, D., Marone, C., and P. Shokouhi, Relating hydro-mechanical and elastodynamic properties of dynamically stressed tensile-fractured rock in relation to applied normal stress, fracture aperture, and contact area. *J. Geophys. Res. Solid Earth*, 129. *doi.org/10.1029/*2023JB027676, 2024.
26. Wood, C., Shokouhi, P., Manogharan, P., Rivière, J., Elsworth, D. and C. Marone, Imaging elastodynamic and hydraulic properties of in-situ fractured rock: An experimental investigation exploring effects of dynamic stressing and shearing, *J. Geophys. Res. Solid Earth*, 126, 10.1029/2020JB021521, 2021.
27. Yu, P., Mali, A., Velaga, T., Bi, A., Yu, J., Marone, C., Shokouhi, P., and D. Elsworth, Crustal permeability generated through microearthquakes is constrained by seismic moment, *Nat. Comm.*, 15:2057, doi.org/10.1038/s41467-024-46238-3, 2024a.
28. Yu, P., Zhu, T., Marone, C., Elsworth, D., and M. Yu, Microseismic Detection on Distributed Acoustic Sensing Arrays using Deep Learning from the Utah FORGE Well 16A (78)-32 Hydraulic Stimulation, *J. Geophys. Res. Solid Earth*, 129, doi.org/10.1029/2024JB029102, 2024b.
29. Yu, J., Eijsink, A., Marone, C., Rivière, J., Shokouhi, P. and D. Elsworth, Role of critical stress in quantifying the magnitude of fluid-injection triggered earthquakes, *Nat. Comm.*, 15:7893, doi.org/10.1038/s41467-024-52089-9, 2024c.
30. Yu, P., Dempsey, D., Rinaldi, A. P., Calibugan, A., Ritz, V. A., & Archer, R., Association Between Injection and Microseismicity in Geothermal Fields With Multiple Wells: Data-Driven Modeling of Rotokawa, New Zealand, and Húsmúli, Iceland. Journal of Geophysical Research: Solid Earth, 128(4), e2022JB025952. 2023.
31. Yu, P. Obermann, A., Rinaldi, A. P., Doonechaly, N.G., Marone, C., Mali, A., Shokouhi, P., and D. Elsworth, Deep Learning Recovers Permeability Evolution from Fluid-Induced Microearthquakes for Hectometer-scale Stimulations, under review Geophysical Research Letters, 2025a.
32. Yu, P., Eijsink, A., Wang, J., Marone, C., and D. Elsworth, Seismic Moment Diagnostic of Crustal Permeability Creation from Centimeter to sub-Kilometer Scales, under review Proceedings of the National Academy of Sciences, 2025b.

11. Project Team and Roles

Marone was the overall project lead and together with Co-PIs Elsworth, Shokouhi, Yang and Zhu they trained and advise the graduate students. Dr. Pengliang Yu served as a postdoctoral fellow and led many aspects of the ML work during Phase 2. The project goals aligned well with expertise and learning objectives of the PI group. The lab experiments and analysis of geothermal data were often done in project team mode, with training of students and project coherency as key goals. Weekly project meetings were helpful in realizing goals and maximizing output. The team had a proven history of success and this project added to that strength. In particular we demonstrated the value of collaboration as a vehicle for interdisciplinary cross fertilization and transformative science.

12. References (see also Research Products of Section 10)

Altman, E., Constrained Markov decision processes with total cost criteria: Lagrangian approach and dual linear program. *Mathematical methods of operations research*, 48(3):387 – 417, 1998.

Berkenkamp, F. , M. Turchetta, A. Schoellig, and A. Krause. Safe model-based reinforcement learning with stability guarantees. In *Advances in Neural Information Processing Systems*, pages 908 – 919, 2017.

Bolton, D. C., Shokouhi, P., Rouet-Leduc, B., Hulbert, C., Rivière, J., Marone, C., and P. A. Johnson, Characterizing acoustic precursors to laboratory stick-slip failure events using unsupervised machine learning, submitted to *Seis. Res. Letts.*, 2018.

Chow. Y., O. Nachum, E. Duéñez-Guzmán, M. Ghavamzadeh, A Lyapunov-based Approach to Safe Reinforcement Learning, abs/1805.07708 CoRR, 2018.

Fang, Y., Elsworth, D., Cladouhos, T.T., Reservoir permeability mapping using microearthquake data, *Geothermics*. 72, 83-100, 2018.

Geibel, P., and F. Wysotzki. Risk-sensitive reinforcement learning applied to control under constraints. *Journal of Artificial Intelligence Research*, 24:81 – 108, 2005.

Holtzman, B. K, Paté, A., Paisley, P., Waldhauser, F. and D. Repetto, Machine learning reveals cyclic changes in seismic source spectra in Geysers geothermal field, *Science Advances*, *4*, eaao2929, 2018.

Hulbert, C., Rouet-Leduc, B., Johnson, P. A., Ren, C. X., Rivière, J., Bolton, D. C., and C. Marone, Machine learning predictions illuminate similarity of fast and slow laboratory earthquakes, In Press. *Nat. Geosc.*, 2018.

Jeanne, P., Rutqvist, J. Rinaldi, A. P., Dobson, P.F., Walters, M. Hartline, C. and J. Garcia, Seismic and aseismic deformations and impact on reservoir permeability: the case of EGS stimulation at the Geysers, California, USA, *J. Geophys. Res. Solid Earth*, 120, 7863–7882, 2015.

Jin, J., Rivière, J., Ohara, Y, and P. Shokouhi, Dynamic acousto-elastic response of single fatigue cracks with different microstructural features: An experimental investigation, *J. App. Phys.* 124, 075303, 2018.

Li, Y., Júlíusson, E., Pálssond, H., Stefánsson, H., and Á. Valfells, Machine learning for creation of generalized lumped parameter tank models of low temperature geothermal reservoir systems, Geothermics, *70*, 62-84, 2017.

Lin, G., and B. Wu, Seismic velocity structure and characteristics of induced seismicity at the Geysers Geothermal Field, eastern California. *Geothermics*, *71*, 225-233, 2018.

Marone, C., Training machines in Earthly ways, *Nature Geosc.,* 11, 301-302, 2018.

Masotti, M., S. Falsaperla, H. Langer, S. Spampinato, and R. Campanini, Application of support vector machine to the classification of volcanic tremor at Etna, Italy, *Geophys. Res. Lett.*, 33, L20304, 2006.

Mudunuru, M. K., Karra, S., Harp, D. R., Guthrie, G. D., and H. S. Viswanathan, Regression-based reduced-order models to predict transient thermal output for enhanced geothermal systems, Geothermics, *70*, 192–205, 2017.

Neil, D., M. Pfeiffer, and S. Liu, Phased LSTM: accelerating recurrent network training for long or event-based sequences, In *Proceedings of the 30th International Conference on Neural Information Processing Systems* (NIPS'16), 2016.

Rasmussen, C., and C. Williams, Gaussian Processes for Machine Learning, the MIT Press, 2006.

Rivière, J., Pimienta, L., Scuderi, M., Candela, T., Shokouhi, P., Fortin, J., Schubnel, A., Marone C., and P. A. Johnson, Frequency, pressure and strain dependence of nonlinear elasticity in berea sandstone, *Geophys. Res. Lett*., 2016.

Rivière, J., Lv, Z., Johnson, P. A., and C. Marone, Evolution of *b*-value during the seismic cycle: insights from laboratory experiments on simulated faults, *Earth and Plan. Sci. Lett.,* 482, 407–413, 10.1016/j.epsl.2017.11.036, 2018.

Ross, A., G.R. Foulger, and B.R. Julian, Source processes of industrially induced earthquakes at the Geysers geothermal area, California, *Geophysics*, 64, 1877-1889, 1999.

Rouet-Leduc, B., C. Hulbert, N. Lubbers, K. Barros, C. J. Humphreys, P. A. Johnson, Machine learning predicts laboratory earthquakes. *Geophysical Research Letters* 44, 9276-9282, 2017.

Rouet-Leduc, B., Hulbert, C., Bolton, D. C., Ren, C. X., Rivière, J., Marone C., Guyer, R. A., and P. A. Johnson, Estimating fault friction from seismic signals, *Geophys. Res. Lett*., 10.1002/2017GL076708, 2018a.

Rouet-Leduc, B., C. Hulbert, and P. A. Johnson, Breaking Cascadia's silence: machine learning reveals the constant chatter of the megathrust, In Press *Nat. Geosc*., 2018b.

Salimzadeh, S., Palusznya, A., Nick, H. M, and R. W. Zimmerman, A three-dimensional coupled thermo-hydro-mechanical model for deformable fractured geothermal systems, *Geothermics*, 71, 212-224, 2018.

Srinivasan, G., Hyman, J. D., Osthus, D. A., Moore, B. A., O'Malley, D. Karra, S., Rougier, E., Hagberg, A. A., Hunter, A. and H. S. Viswanathan, Quantifying topological uncertainty in fractured systems using graph theory and machine learning, *Nature Scientific Reports*, *8,* 11665, 2018.

SigurÐardottir, S. R., Valfells, A., Pálsson, H., and H. Stefansson, H., Mixed inter optimization model for utilizing a geothermal reservoir, *Geothermics*, 55, 171–181, 2015.

Shokouhi, P., J. Rivière, C. R. Lake, P.Y. Le Bas, and T.J. Ulrich, Dynamic acousto-elastic testing of concrete with a coda-wave probe: comparison with standard linear and nonlinear ultrasonic techniques, *Ultrasonics* 81, 59-65, 2017.

Viswanathan, H. S., Hyman, J. D., Karra, S., O'Malley, D., Srinivasan, S., Hagberg, A., and G. Srinivasan, Advancing graph-based algorithms for predicting flow and transport in fractured rock. *Water Resources Research*, *54*, 6085–6099, 2018.

Yang, J., S. Draper, and R. Nowak, Learning the interference graph of a wireless network, *IEEE Trans. on Signals and Information Processing over Networks*, 3(3), 631-642, 2017.

Yu, C., Vavryčuk, V., Adamová, P., and M. Bohnhoff, M, Moment tensors of induced microearthquakes in The Geysers geothermal reservoir from broadband seismic recordings: Implications for faulting regime, stress tensor, and fluid pressure. *J. Geophys. Res.: Solid Earth*, 123, 2018.

Zhou, R., C. Gan, J. Yang and C. Shen, Cost-aware Cascading Bandits, *The 27th International Joint Conference on Artificial Intelligence (IJCAI 2018)*, Stockholm, Sweden, July 2018.

Zhu, T., Ajo-Franklin, J., Daley, T. and C. Marone, Dynamics of geologic CO_2 storage and plume motion revealed by seismic coda waves, Submitted to PNAS, 2018a.

Zhu T., Sun J., Gei D., Carcione J.M., P. Cance, and C. Huang, Hybrid multiplicative time-reversal imaging reveals the evolution of microseismic events: Theory and field data tests, submitted to *Geophysics,* 2018b.